Mesoscopic Orientational Order Accompanies the Slow Dynamics of a Two-Dimensional Supercooled Liquid

Andrew Ton

A thesis submitted for the degree of

Sc.B. Honors, Chemical Physics

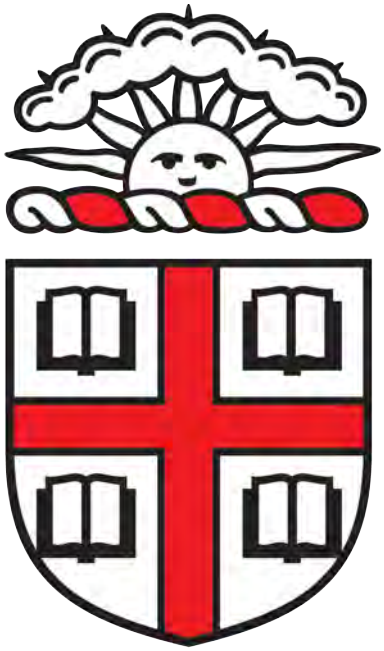

Brown University

April 2020

Advisor: Professor Richard Stratt

Abstract

We introduce the 2dLW model, which successfully captures kinetic fragility as the liquid is supercooled. The supercooled liquid suffers a glass transition around $0.30 < Tg^* < 0.35$, after which the fragile dynamics crossover to strong, Arrhenius-type activated dynamics. The Vogel-Fulcher-Tamman law, which models fragile dynamics, predicts $T_o \approx 0.30$. Much like how pseudonematic domains result in slow, power-law decay of orientational time correlation functions in liquid crystals, we conjecture that the slow, fragile dynamics of the 2dLW supercooled liquid are caused by molecular-orientational hexatic domains. This is in contrast to literature expectations of the general unimportance of structure to glassy dynamics. Our findings of ordered domains suggest a microscopic mechanism behind the famous slow dynamics of supercooled liquids. 2dLW domains are mesoscopic, with lengthscale ranging from the length of a few molecules to the length of dozens of molecules. Finite-size-scaling arguments show that the structural order is truly mesoscopic rather than long-range or quasi-long-range. We find that supercooling gives rise to two nearest-neighbor lengthscales with different orientational ordering associated with each length. In summary, we find in a two-dimensional supercooled liquid and glass unexpected molecular-orientationally ordered structures that we believe are structural signatures of glassy dynamics.

Acknowledgements

I am thankful for the mentorship of my advisor, Professor Richard Stratt, who has taught me what it means to be a scientist. This thesis was also made possible by my friends' unflagging support, even when I disappear for long periods of time to study. The process of research would be much less pleasant and productive without the company and conversation of the various members of our research group. I have fond memories of discussions with Vale Cofer-Shabica, Yan Zhao, Yichen Chai, Lefteris Mainas, Dawei Si, Sam Oaks-Leaf, and many others.

Contents

Abstract i

Acknowledgements ii

1 Introduction **2**

1.1 Supercooled liquids and glasses 3

1.2 Liquid crystals 4

1.2.1 Order and disorder 4

1.3 Slow dynamics 8

1.4 Two-dimensional systems 11

1.4.1 Mermin-Wagner effect - long-wavelength fluctuations 11

1.4.2 Cage-relative coordinates 12

1.4.3 Note on bond-orientational order 13

1.5 "Phase diagram" 13

2 Method - Computer Simulations of Liquids **17**

2.1 Using computers to solve liquid problems 17

2.1.1 A brief review of theoretical progress 18

2.2 Velocity Verlet algorithm 19

2.3 Numerical model (2dLW) 20

2.3.1 The Lewis-Wahntröm model in three dimensions 20

2.3.2 The Lewis-Wahnström model in two dimensions 21

2.4 Simulation parameters . . . 22
2.5 Protocols . . . 24
2.5.1 Beginning the simulation . . . 24
2.5.2 Simulated Annealing . . . 25
2.5.3 Equilibrating and taking data . . . 27
2.5.4 Taking averages . . . 29

3 Supercooled dynamics **30**
3.1 Correlation function . . . 31
3.2 Autocorrelation and mean square displacement . . . 32
3.3 Phenomenology . . . 36
3.4 Amorphous solid . . . 37

4 Mesoscopic structure **47**
4.1 Hexatic molecular orientational order . . . 48
4.1.1 How about m-adic order for m $\neq$ 6? . . . 50
4.1.2 Literature precedent . . . 50
4.2 Mesoscopic structure . . . 53
4.2.1 Neither macroscopic nor quasi-long-range order . . . 55
4.3 Structural domains . . . 60
4.4 Local order . . . 61
4.4.1 Note on cavitation . . . 64
4.5 Bond-orientational order . . . 66

5 Conclusion **70**

A Results from other trimer models **73**

CHAPTER 1

Introduction

One of the current problems in condensed matter is understanding the liquid state. Studying the physics of liquids is particularly challenging. Liquid systems are disordered and thus lack the symmetries that facilitate solid state theory. Gas theory is not applicable either because particle interactions are fundamental to liquid properties. Our technique is to use statistical mechanics and numerical simulation to help us learn more about liquids.

Supercooled liquids and liquid crystals are two subsets of liquids examined in this thesis. Both have unusual properties. Harnessing the anomalously slow dynamics of supercooled liquids and glasses led to revolutionary advances in microscopy (see Nobel Prize in Chemistry, 2017) and continues to find application in fields like food science. [1] [2] These applications are in addition to the ubiquity of glass as an engineering and optical material. On the other hand, liquid crystals flow like ordinary liquids yet attain symmetries otherwise found only in crystals. Liquid crystals' unique optical properties enabled the invention of liquid crystal displays (LCDs) while their symmetry properties endow materials like Kevlar with the integrity to stop bullets. [3] This thesis introduces a numerical model for a supercooled, glassforming system that also attains liquid crystalline order in its supercooled state. Special attention will be paid to the unique nature of the liquid crystalline order and the dynamics

of the supercooled liquid.

1.1 Supercooled liquids and glasses

Supercooled liquids are liquids cooled below their freezing temperature. As such, they have a thermodynamic preference for being crystal. In other words, a crystal structure below the freezing point will have a lower free energy than its corresponding liquid structure. Then in order for a liquid to become supercooled, it must find a way to avoid crystallization. This is not the only concern when preparing a supercooled liquid sample. In fact, supercooled liquids have another option when cooled far past their freezing points. Here, a competition on the atomic level between two processes in a liquid becomes relevant: crystal nucleation time and liquid relaxation time. There is an art to the science of preparing laboratory (and numerical, in our case) supercooled liquids. [4] One starts with an ordinary liquid and cools it according to some cooling schedule. If the cooling rate is too slow, then the atoms have ample time and opportunity to form a stable crystal nucleus because it is thermodynamically favorable to do so. On the other hand, if the cooling occurs on a timescale quicker than the liquid's relaxation time, then the system will fail to equilibrate and undergo dynamic arrest. This forms an amorphous solid - what we call glass.

The delicacy of preparing a supercooled liquid comes from its thermodynamic metastability. The supercooled liquid can remain liquid over finite timescales if undisturbed. However, the supercooled liquid would actually rather be anything other than liquid. It negotiates between two choices of solids: crystal and glass. Of interest is the supercooled liquid at the point where it chooses glass over crystal. This is the deeply supercooled liquid, a regime in which liquid dynamics become so slow that it becomes impossible for a crystal nucleus to grow. We are concerned with the anomalous viscous slowdown of dynamics in deeply supercooled liquids.

1.2 Liquid crystals

Soft matter as a subfield of condensed matter was popularized by the celebrated work of de Gennes and other scientists in the 1970s. [5] Compared to the light speed and high energy of particle physics, the cosmic scales of astrophysics, and the ultracold temperatures of hard condensed matter physics, soft matter physics can be understood as the study of systems with familiar lengthscales that evolve on familiar timescales. The physics of soft matter is many-body in nature, with lengths as short as a few atoms or as long as thousands of molecules. The interesting physics occurs over nanoseconds or milliseconds - timescales on which very interesting (or very slow) processes become relevant.

Liquid crystals are no exception to these lengthscales and timescales. Such liquid crystal systems form a considerable number of distinct liquid phases, of which we will concern ourselves with just two - the isotropic and nematic liquid crystals. The *nematic* phase of liquid crystals draws the closest analogy to the order we discover and describe in this thesis. The following exposition draws from de Genne's book, *The physics of liquid crystals.* [6]

1.2.1 Order and disorder

We consider a system liquid if knowledge about one molecule's properties does not betray any information about the properties of another molecule when sufficiently far from the original molecule. In such systems we say that correlation is lost over some finite lengthscale. The loss of orientational correlation over finite distances is a property that we call "isotropic". Similarly, we refer to a liquid with positional disorder as "homogeneous".

Ordinary liquids are isotropic. Liquid crystals in their various ordered phases are not. Instead, constituent molecules of nematic liquid crystals have liquid-like positional disorder and crystal-like molecular-orientational order. This liquid-like positional disorder means that the liquid crystal loses positional correlation over finite distances. However, there remains macroscopic orientational order, meaning that the orientation of molecules in one portion of

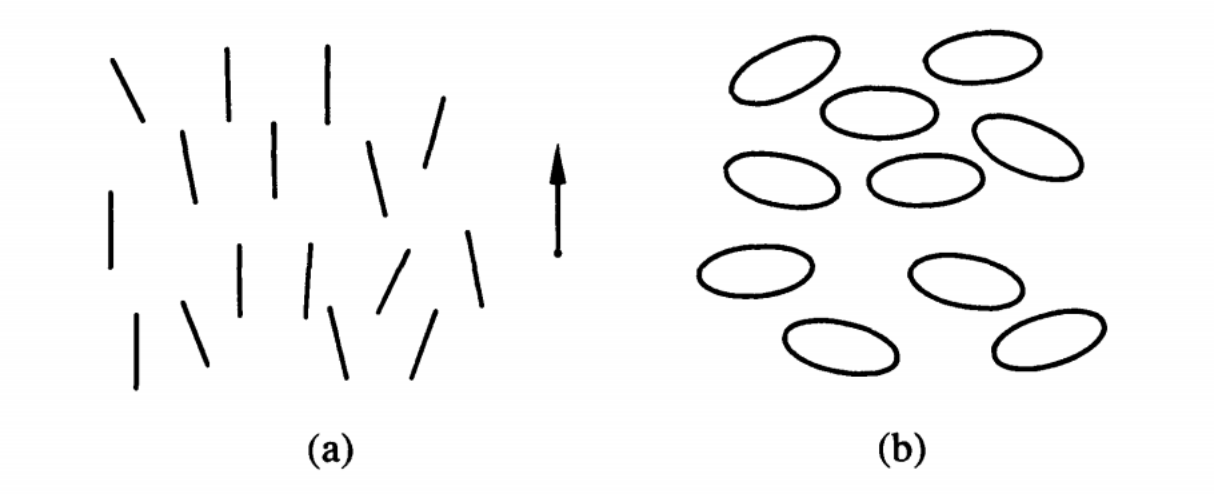

Figure 1.1: Nematic liquid crystal molecules represented as (a) rods and (b) disks. Figure from reference [6].

a sample gives information about orientations of molecules in any other part of the sample.

The nature of this molecular-orientational order is that molecules, on average, will favor being parallel to some common axis called the *director*. To facillitate the study of nematic order, one typically defines a nematic order parameter tensor, $\mathbf{Q}_{\alpha\beta}$. Since we work with a two-dimensional system for this thesis, $\mathbf{Q}_{\alpha\beta}$ reduces to a matrix $\mathbf{Q}_m$. These are given as:

$$\mathbf{Q}_m = \begin{pmatrix} Q_1^{(m)} & Q_2^{(m)} \\ Q_2^{(m)} & -Q_1^{(m)} \end{pmatrix} \tag{1.1}$$

$$Q_1^{(m)} = \frac{1}{N}\sum_{j=1}^{N} \cos\, m\theta_j \tag{1.2}$$

$$Q_2^{(m)} = \frac{1}{N}\sum_{j=1}^{N} \sin\, m\theta_j \tag{1.3}$$

where N is the number of particles and θ_j is the angle between molecule j and any lab-frame axis.

We parametrize the order parameter matrix using an integer m with great foresight. The nematic order parameter matrix with $m = 2$ captures the two-fold molecular-orientational

order of nematic liquid crystals: molecules that prefer being parallel or antiparallel to the director. We generalized to m-fold order because our model system displayed 6-fold order, and we were interested in seeing what kinds of order showed up in similar models.

Because $\mathbf{Q}_m$ is traceless, we can quickly deduce that $\mathbf{Q}_m$ has two eigenvalues $\pm\lambda_m$. To capture the extent of m-fold orientational order in terms of single particle contributions, we define a complex quantity s_m:

$$s_m = \frac{1}{N}\sum_{j=1}^{N} e^{im\theta_j} \tag{1.4}$$

where θ_j is the angle between the orientation vector of molecule j and an arbitrary lab-frame axis. s_m is related to the eigenvalue λ_m by

$$\begin{aligned}
\lambda_m^2 &= -\mathrm{det}\mathbf{Q}_m \\
&= Q_1^{(m)} + Q_2^{(m)} \\
&= -\frac{1}{N^2}\sum_{j,k=1}^{N}[\mathrm{cos}m\theta_j\mathrm{cos}\theta_k + \mathrm{sin}\theta_j\mathrm{sin}\theta_k] \\
&= \frac{1}{N^2}\sum_{j,k=1}^{N}\mathrm{cos}m(\theta_j - \theta_k) \\
&= |s_m|^2
\end{aligned}$$

This allows us to write a simple formula for the m-fold orientational order parameter $|s_m|$:

$$|s_m| = |\frac{1}{N}\sum_{j=1}^{N} e^{im\theta_j}| = \sqrt{\frac{1}{N^2}\sum_{j,k=1}^{N}\mathrm{cos}\ m(\theta_j - \theta_k)} = \lambda_m \tag{1.5}$$

Note that s_m is a complex number which takes on the value 1 in a system with perfect m-fold orientational order and vanishes in the macroscopic ($N \to \infty$) limit for disordered systems.

Similarly, we can define for each configuration a preferred axis of alignment, $\hat{n}$, called the director. The eigenvector of $\mathbf{Q}_2$ is the director for a configuration with nematic order,

but the eigenvector of $\mathbf{Q}_6$ is not the director for a configuration with hexatic order. We will prove that the eigenvector of $\mathbf{Q}_m$ is the director for $m = 2$, but not for $m \neq 2$.

Proof. Let $\hat{\Omega}_j = \begin{pmatrix} \cos\theta_j \\ \sin\theta_j \end{pmatrix}$, where $\hat{\Omega}_j$ is the unit orientation vector of molecule j.

Certainly we can express the top left element of $\mathbf{Q}_m$ in terms of an argument ϕ. The traceless property of $\mathbf{Q}_m$ determines the bottom right element. The determinant must be -1, which determines the top right and bottom left elements. Thus we can express $\mathbf{Q}_m$ in terms of an argument ϕ:

$$\mathbf{Q}_m = \begin{pmatrix} cos\phi & sin\phi \\ sin\phi & -cos\phi \end{pmatrix}$$

we have its positive eigenvector:

$$\hat{q}_+ = \begin{pmatrix} cos\theta_o \\ sin\theta_o \end{pmatrix}$$

such that

$$\mathbf{Q}_m \hat{q}_+ = \hat{q}_+$$

.

Then

$$\begin{pmatrix} cos\phi cos\theta_o + sin\phi sin\theta_o \\ sin\phi cos\theta_o - sin\theta_o cos\phi \end{pmatrix} = \begin{pmatrix} cos\theta_o \\ sin\theta_o \end{pmatrix}$$

.

Using trigonometric identities, this simplifies to

$$\begin{pmatrix} cos(\phi - \theta_o) \\ sin(\phi - \theta_o) \end{pmatrix} = \begin{pmatrix} cos\theta_o \\ sin\theta_o \end{pmatrix}$$

So $\theta_o = \phi/2$.

Consider

$$\begin{aligned}
S &= \frac{1}{N}\sum_{j=1}^{N} T_m(\hat{\Omega}_j \cdot \hat{n}) \\
&= \frac{1}{N}\sum_{j=1}^{N} cos(m(\theta_j - \theta_o)) \\
&= \frac{1}{N}\sum_{j=1}^{N} (cosm\theta_o cosm\theta_j + sinm\theta_o sinm\theta_j) \\
&= cosm\theta_o \frac{1}{N}\sum_{j=1}^{N} cosm\theta_j + sinm\theta_o \frac{1}{N}\sum_{j=1}^{N} sinm\theta_j \\
&= \begin{pmatrix} cosm\theta_o \\ sinm\theta_o \end{pmatrix} \cdot |s_m| \begin{pmatrix} cos\phi \\ sin\phi \end{pmatrix} \\
&= |s_m| cos(\phi - m\theta_o)
\end{aligned}$$

.

Thus $S = |s_m|$ if and only if $\theta_o = \phi/m + 2\pi l$, l an integer.

We saw previously that $\theta_o = \phi/2$, so we conclude that $S = |s_m|$ only when $m = 2$. This proves that the eigenvector corresponding to the positive eigenvalue of $\mathbf{Q}_2$ is the director. □

For $m = 6$ and θ_o defined as above,

$$\hat{n} = \begin{pmatrix} cos3\theta_o \\ sin3\theta_o \end{pmatrix} \tag{1.6}$$

1.3 Slow dynamics

We will explore the characteristic slow dynamics of supercooled liquids further in Chapter 3. The salient feature of this slowness is the separation of timescales between ballistic and diffusive molecular motions. The short-time ballistic motion results in what is called β relaxation, whereas the hydrodynamic self-diffusive motion is called α relaxation. This phe-

nomenon of two-step relaxation is a result of molecules becoming trapped in a "cage" formed by neighboring molecules on intermediate timescales, but the cage is sufficiently sparse to permit the eventual diffusion of the molecule into the rest of the system. This temporary caging effect is referred to as "transient localization", and it is a distinct signature of deeply supercooled liquids. We can see the different relaxations and the transient localization in a quantity called the mean square displacement $\Delta r^2(t)$ (see Figure 1.2):

$$\delta r_i(t) = r_i(t) - r_i(0) \tag{1.7}$$

$$\Delta r^2(t) = \left\langle \frac{1}{N} \sum_{i=1}^{N} (\delta r_i(t))^2 \right\rangle \tag{1.8}$$

where i indexes the molecules, and r_i is the position vector of the i-th molecule. The mean square displacement allows us to quantify relaxation processes in liquids. The diffusion constant, which we explain further in Chapter 3, can also be calculated from the mean square displacement. The temperature dependence of this constant is of great interest as a way to touch base with theories of the glass transition which make predictions about the scaling behavior with temperature. [7]

The Fayer group at Stanford had an interesting insight that supercooled liquids and liquid crystals have similar temperature dependence of their dynamics. [8] They discovered using orientational time correlation functions that both supercooled liquids and liquid crystals experience a temperature-independent power law decay, then a dynamical crossover regime, and finally a temperature-dependent exponential decay. Their study conjectures that because the slow dynamics of isotropic liquid crystals correspond so closely to the slow dynamics of supercooled liquids, one can expect a common microscopic explanation for the slow dynamics. It is known that isotropic liquid crystals actually form structures called "pseudonematic" domains, which are the origin of the slowness in a liquid crystal's isotropic phase. For this reason, Fayer suggests investigation into microscopic structures of supercooled liquids as a way forward in understanding supercooled slow dynamics. This thesis builds on this

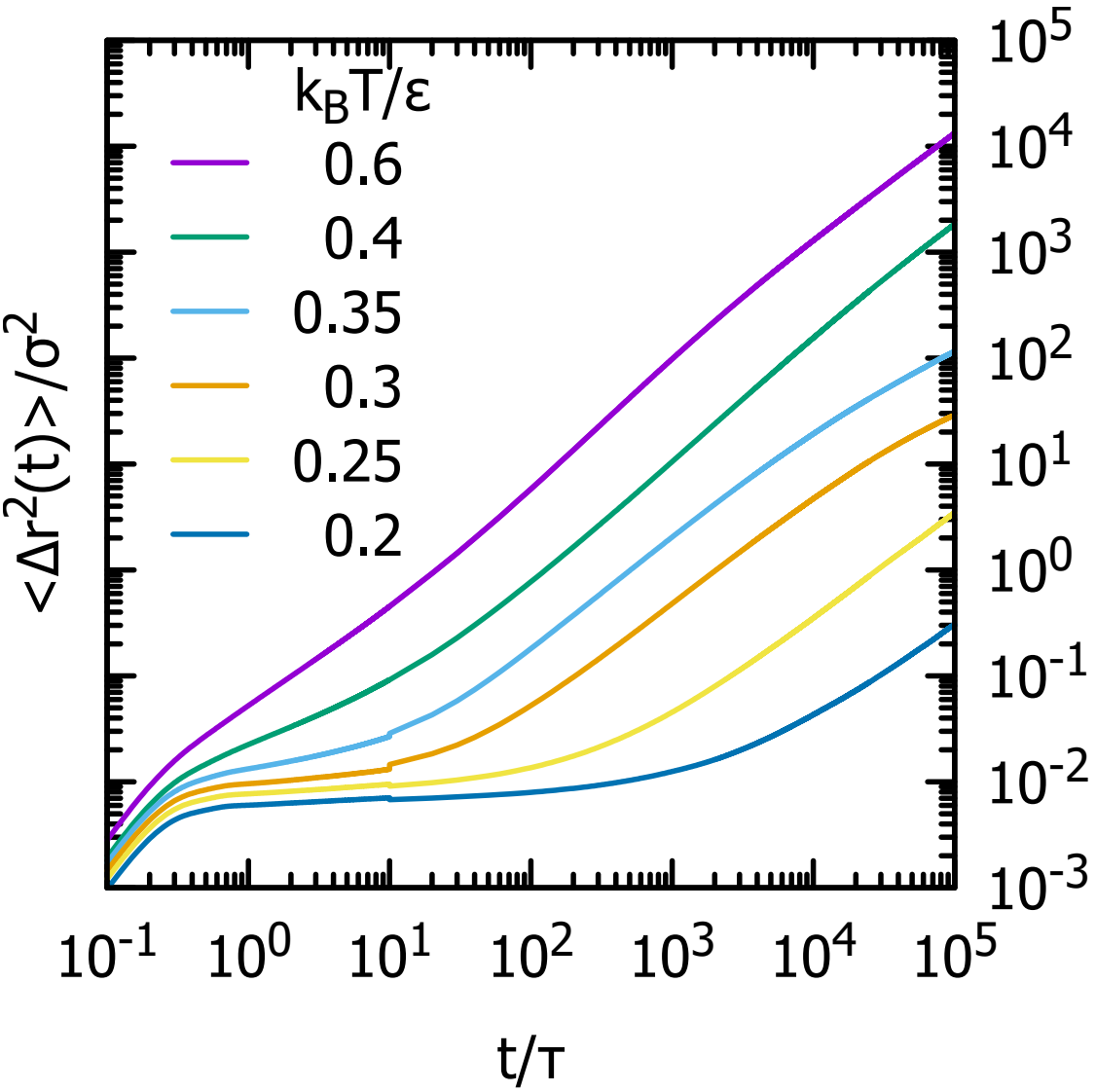

Figure 1.2: Mean square (cage-relative) displacement of systems of N=800 2dLW molecules. Averages are taken over 2×10^5 trajectories. τ is on the order of 10^{-12} seconds, and $\epsilon/k_B = 600K$. Observe the ballistic regime with timescale less than τ and slope 2, a plateau (lengthening with decreasing temperature) with slope 0 indicating the separation of β relaxation and α relaxation, and an eventual diffusive regime with slope 1.

conjecture by examining mesoscopic structures in a deeply supercooled liquid.

1.4 Two-dimensional systems

In 2015, a paper by Flenner and Szamel arrived at a disturbing conclusion about fundamental differences between dynamical results in two and three dimensions. [9] Their study discovered that transient localization was absent in two dimensional simulations of a binary glassformer. Their model also lacked dynamical heterogeneity, another signature of deeply supercooled liquids in which dynamically active molecules tend to be near other dynamically active molecules whereas the rest of the system is inert. Since we study 2d supercooled liquids, it is important that we acknowledge Flenner and Szamel's findings about fundamental differences between supercooled dynamics in 2d and 3d.

There is a growing body of work on 2d dynamics in spite of Flenner and Szamel's work which show that 2d dynamics are actually not so different than 3d dynamics. A number of papers came out to address Flenner and Szamel's results. [10] [11] [12] They describe the Mermin-Wagner theorem, a well-known theoretical result that separates three dimensional space from lower dimensional spaces, and a clever coordinate system that permits measurements of translational correlations by correcting for the Mermin-Wagner effect. The takeaway from these papers is a solid defense of the theoretical soundness of studying supercooled dynamics in two dimensions.

1.4.1 Mermin-Wagner effect - long-wavelength fluctuations

The Mermin-Wagner theorem states that continuous symmetries cannot be broken in systems with short-range interactions in two or fewer dimensions at finite temperature. [13] This led many to doubt the existence of 2D crystals, which would break translational symmetry and violate the theorem. The mechanism by which the crystalline lattice in low dimensional systems is destroyed is referred to as long-wavelength or Mermin-Wagner fluctuations.

It is these long-wavelength fluctuations predicted by the Mermin-Wagner theorem that quite literally unsettle two-dimensional studies of dynamics whether experimental, numerical, or theoretical. Due to the long-wavelength nature of the fluctuations, the associated timescale of these fluctuations is very slow. In fact, the long-wavelength fluctuations are easily mistaken for diffusive α relaxation processes - which is likely what Flenner and Szamel unknowingly reported on in their paper. Fortunately, the many workers who addressed Flenner and Szamel's results came up with a solution to dynamical studies in light of long-wavelength fluctuations: we can move to a coordinate system that takes into account these long-wavelength fluctuations.

1.4.2 Cage-relative coordinates

A simple modification to translational correlation functions and similar quantities like the mean square displacement allows us to see past the long-wavelength fluctuations. While the mean square displacement is given by Equation 1.7, one can make the following change to define the mean square cage-relative displacement:

$$\Delta r^2_{CR}(t) = \left\langle \frac{1}{N} \sum_{i=1}^{N} (\Delta r_{i,CR}(t))^2 \right\rangle \tag{1.9}$$

where

$$\Delta r_{i,CR}(t) = \delta r_i(t) - \frac{1}{N_{nn}} \sum_{j \in \{n.n.\}_i} \delta r_j(t) \tag{1.10}$$

where $\{n.n.\}_i$ is the set of indices for the neighbors of molecule i.

The cage-relative displacement given by Equation 1.10 works to undo the effects of long-wavelength fluctuations. Instead of measuring displacement of a molecule, we can instead measure the displacement of that molecule relative to the displacements of its neighboring molecules, i.e. its cage. Since the fluctuations have long wavelengths, the cage of any given molecule and the molecule itself will move together in a wave motion. Then by only measuring displacement relative to a particle's cage, we can recover the true dynamics independent

of long-wavelength processes. Thus, cage-relative coordinates rescue two-dimensional dynamical studies from the Mermin-Wagner effect. The mean square displacement in Figure 1.2 is in fact cage-relative displacement. For comparison between cage-relative and ordinary mean square displacement, see Figure 1.3.

1.4.3 Note on bond-orientational order

Two-dimensional liquids are famous for "bond-orientational" order. [14] This is explained by KTHNY theory, which studies how topological defects lead to continuous liquid-liquid phase transitions. In particular, there is a 2d hexatic phase where particles in a system have hexatic bond-orientational order. A longer discussion of bond-orientational order can be found in Section 4.5. One of the essential findings about our model system is that it has what we call *hexatic* molecular-orientational order, where molecules prefer to align their molecular orientations along six preferred directions. Referring to *hexatic* order (emphasis on omitting "molecular-orientational") in the case of two-dimensional systems usually one means hexatic bond-orientational order. This should not be confused for our finding of hexatic molecular-orientational order, which is a new idea.

1.5 "Phase diagram"

To work in the constant-NVE ensemble, we fixed in our simulations the number of particles N, simulation box size L^2, and total mechanical energy E. The relevant thermodynamic parameters are density ($\rho = N/L^2$) and temperature (proportional to average kinetic energy). We will use dimensionless temperature T^* and dimensionless density ρ^* paremeters whose exact definitions will become meaningful when the parameters of our model are defined in Chapter 2. For this thesis, all simulations were conducted at constant density $\rho^* = 0.25$.

There are three distinct regimes: high temperature, intermediate temperature, and low temperature. At high temperatures ($T^* \geq 0.45$) we have an ordinary isotropic liquid char-

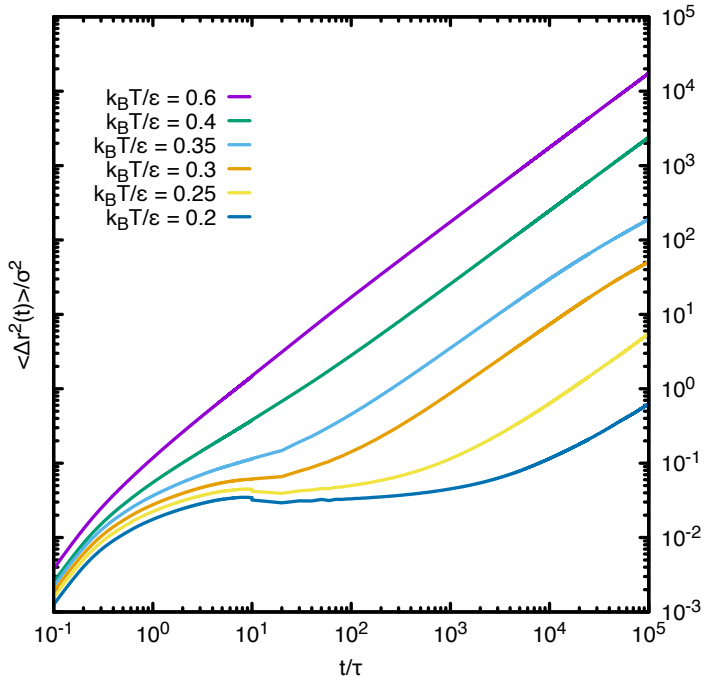

(a) Mean square displacement of the N=800 2dLW system.

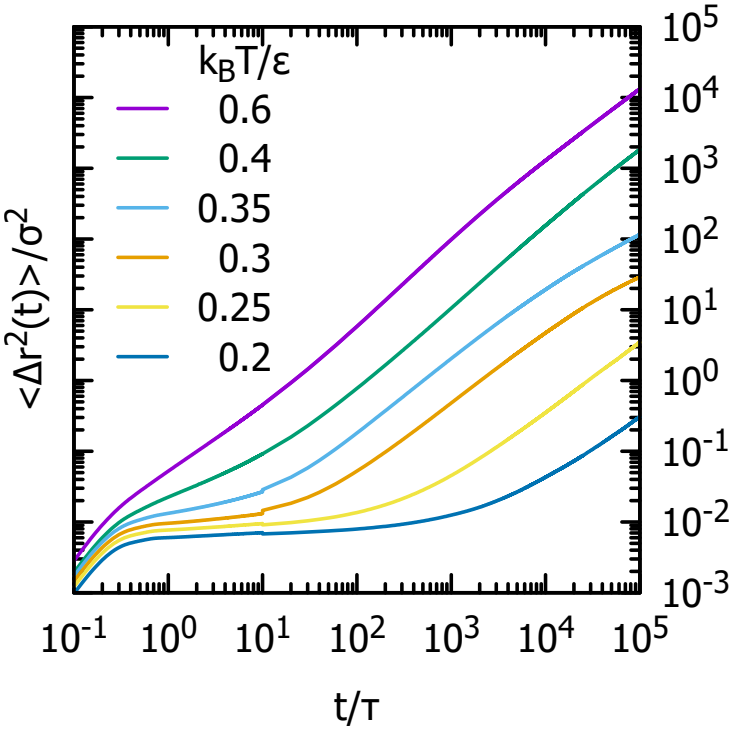

(b) Cage-relative mean square displacement of the N=800 2dLW system.

Figure 1.3:

acterized by simple diffusion, rapid relaxation processes, and weak temperature dependence of diffusion constant. These are the expected characteristic features of ordinary liquids. We learn about diffusion through the mean square displacement (Figure 1.2) and a study of diffusion constant versus temperature (Figure 3.3). Relaxation processes are studied similarly, using the mean square displacement as well as orientational correlation functions (Figure 3.2, 3.1).

At intermediate temperatures ($0.35 \leq T^* < 0.45$), we have a fragile supercooled liquid state with higher density than the isotropic liquid, mesoscopic six-fold molecular-orientationally ordered domains, Vogel-Fulcher temperature dependence of diffusion constant, and dramatic slowing down of orientational dynamics. The domains are pictured in Figure 4.5. The property of kinetic fragility in the supercooled liquid is modeled by a fitting equation called the Vogel-Fulcher-Tamman law (VFT). The Vogel-Fulcher form predicts $T_o \approx 0.30$ (Figure 3.3), where T_o is a finite temperature at which relaxation times are predicted to diverge and the diffusion constant to precipitously plummet. We show that the domains are mesoscopic as opposed to long-range or pseudo-long-range in Chapter 4 using a finite-size-scaling study (Figure 4.8). We also examine the local order in Figure 4.11, Table 4.3, and Figure 4.5. We did not know *a priori* that our model would form a supercooled liquid, so the fact that the VFT law is a good fit helps us confirm we have a supercooled liquid, among other dynamical and structural factors discussed in Chapter 3. It is very surprising that mesoscopic domains form in the supercooled liquid. Supercooled liquids are understood to be structurally indistinguishable from ordinary liquids, yet in our model we establish that the supercooled liquid attains domains of six-fold molecular-orientational order. This is a shocking break from the expected behavior of supercooled liquids. Additionally, the six-fold molecular-orientational order itself is very novel, as we have not been able to find any remark in the literature of six-fold orientational order in physical systems (with a notable exception by the Mason group at UCLA). The Mason group finds six-fold molecular-orientational order in equilateral triangles, and makes no mention of any supercooling in their experiments. [15] We note that

our particles do not have the symmetries of a triangle, nonetheless an equilateral triangle. It is very surprising to see molecular-orientational order with a mesoscopic lengthscale, and even more so since our model has a particle geometry that we would not normally expect to support molecular-orientational order.

At low temperatures ($T^* < 0.35$) the system has undergone a glass transition and is now amorphous solid. This glass has slightly higher density still than the supercooled liquid, with more numerous and shorter-lengthscale six-fold ordered mesoscopic structures. The directors of these numerous mesoscopic structures vary significantly from domain to domain, resulting in a drastic decrease in global orientational order parameter (Figure 4.2, 4.5). The temperature dependence of the diffusion constant is Arrhenius (Figure 3.3), indicating that dynamics are dominated by activated events. Relaxation processes are frozen out - α relaxations have negligible magnitude in the mean square displacement (Figure 1.2) and orientational correlations (Figure 3.2, 3.1) do not decay over the timescales of our simulations. It is interesting that the mesoscopic structures persist through the supercooled liquid and into the glass. That the structure of the supercooled liquid and the glass are similar is no surprise, but normally it is because both are structurally similar to ordinary liquids!

CHAPTER 2

Method - Computer Simulations of Liquids

This chapter will cover the numerical techniques employed to model our supercooled liquid system. After briefly discussing the paradigm of computer simulation in modern scientific research, we introduce the particular numerical model that we use to model supercooled liquid behavior. The chapter explains our reasoning in the design and choice of this model, and goes into explicit detail regarding the various protocols and routines involved in preparation of the supercooled liquid and calculation of the correlation functions. The exposition of this chapter pulls strongly from Allen and Tildesley's excellent reference on simulation, *Computer Simulations of Liquids (ed. 2)*. [16]

2.1 Using computers to solve liquid problems

Computer simulation is a relatively new addition to the paradigm of science, beginning in the 1950s at Los Alamos. Two classes of algorithms come to mind when considering computer simulation. There are the Monte Carlo algorithms which broadly rely on probability to generate thermodynamic data, and the Molecular Dynamics algorithms which use finite-difference methods to solve the differential equations dictated by Newton's equations

of motion. To study the dynamics of supercooled liquids, one uses the latter method of molecular dynamics. Monte Carlo simulations do not give microscopically correct dynamics, whereas Molecular Dynamics simulations generate accurate trajectories and permit the computation of dynamical observables.

2.1.1 A brief review of theoretical progress

Theoretical progress is guided by attempting to model and predict actual supercooled liquid behavior. For example, take Mode Coupling Theory (MCT), the only first-principles theory of the glass transition. [17] MCT comes with impressive success at predicting scaling behaviors of supercooled liquids at higher temperatures. As temperatures approach the glass transition, MCT makes incorrect predictions including mistakenly predicting the glass transition to occur at a higher temperature than in experiment. [7] Further, MCT fails to predict a phenomenon called dynamical heterogeneity, an important signature of deeply supercooled dynamics. For these reasons, MCT is regarded as a successful theory of moderately supercooled liquids while its low-temperature predictions must be considered with great caution. Our simulation work fits into this paradigm by providing a virtual laboratory where we can test theories and probe our system for higher resolution data than experimentally accessible.

Other than MCT, the two dominant approaches to glass theory use Random First Order Transition (RFOT) theories and dynamical facilitation. The reader is encouraged to read Berthier and Biroli's review on glass theories as an introduction to these ideas. [7] RFOT is a collection of mean-field theories of the glass transition that study the free energy landscapes in model systems as they approach the glass transition. It has been successful in predicting certain thermodynamic signatures of the glass transition, such as vanishing entropy and discontinuity in the specific heat. For our purposes, it is important that certain RFOTs predict VFT law divergence in relaxation times. [18] We show in Figure 3.3 that at intermediate temperatures, our model supercooled liquid has diffusion constant following the VFT law. When existing theories predict results in numerical simulations like ours, it

is very important to examine the microscopic mechanisms underlying the theory. This is particularly important for mean-field models like RFOTs, where the theory may not teach us everything about the actual processes that give rise to the many interesting phenomena of supercooled liquids.

Dynamical facilitation is another approach that focuses solely on the dynamics of particles as responsible for the glass transition. This can be viewed in opposition to RFOTs and MCT which use mean-field theories. Dynamical facilitation gives rise to kinetically constrained models (KCMs), for which we refer the reader to Berthier and Biroli's review. [7] In short, the KCM approach uses the idea that in viscous liquids, a local relaxation event will propagate through a system. KCMs assert that for a region of a sample to be mobile, it must be adjacent to another mobile region. This is a strong requirement that captures an aspect of glassy mobility at the expense of ignoring other mechanisms of mobility. KCMs also predict a VFT divergence in relaxation times, but in this case also provide a responsible mechanism, albeit an unphysical requirement about mobility propagation. As a purely dynamical theory, KCMs have been the most successful in modeling dynamical heterogeneity.

2.2 Velocity Verlet algorithm

Newton's equations of motion describe the classical dynamics of particles as a system of differential equations. Solving these equations in practice is generally impossible for systems of more than two particles. The advent of computers made it possible to apply numerical approximation algorithms to iteratively and approximately solve difficult or impossible systems of equations. Of these algorithms, we will focus on a particular finite-difference algorithm called Velocity Verlet.

The Velocity Verlet algorithm is simple and accurate. It takes the positions and velocities of each molecule in a state at a certain time t, and computes the positions and velocities at a new time $t + \delta t$. [16] The equations for this algorithm are as follows:

$$\mathbf{v}(t + \frac{1}{2}\delta t) = \mathbf{v}(t) + \frac{1}{2}\delta t\ \mathbf{a}(t) \tag{2.1}$$

$$\mathbf{r}(t + \delta t) = \mathbf{r}(t) + \delta t\ \mathbf{v}(t + \frac{1}{2}\delta t) \tag{2.2}$$

$$\mathbf{v}(t) = \mathbf{v}(t + \frac{1}{2}\delta t) + \frac{1}{2}\delta t\ \mathbf{a}(t + \delta t) \tag{2.3}$$

Each successive equation in this algorithm depends on the last, and the last equation requires one to know the forces on the molecule at the next timestep. The right hand side of each equation is a truncated Taylor expansion of the left hand side. As such, the global error of this algorithm depends on δt^2 (the local error depends on δt^4). We use a small δt to minimize this. Despite Velocity Verlet's reputation as a numerically stable algorithm that produces accurate solutions, we took precautions to check the accuracy of the algorithm. This was as simple as confirming conservation of total mechanical energy in a variety of model systems and simulating simple systems with known analytical expressions for certain correlation functions.

2.3 Numerical model (2dLW)

2.3.1 The Lewis-Wahnström model in three dimensions

The most important feature of a supercooled liquid is its ability to avoid crystallization. Ortho-terphenyl is a molecule that excels at remaining amorphous when cooled, leading Lewis and Wahnström to introduce a simple model for a supercooled liquid based on ortho-terphenyl. [19] The Lewis-Wahnstrom model (3dLW) is a popular choice of glassformer for three-dimensional studies. We report on a few key 3dLW studies. In Lewis and Wahnström's original paper introducing and testing the model, they find that their 3dLW model is a fragile glassforming fluid, as is laboratory ortho-terphenyl after which 3dLW is modeled.[19] Later studies find that the temperature dependence of the diffusion constant in 3dLW is well

predicted by Mode Coupling Theory at high temperatures, and a crossover is observed to activated dynamics at lower temperatures. [20] [21] We will make our connection to these discussions in Chapter 3. Finally, Pedersen, Hudson, and Harrowell published a study on the crystallization of 3dLW that finds that the supercooled liquid typically crystallizes after about 100 times the relaxation time of the supercooled liquid. [22] In other words, it is not as difficult to crystallize 3dLW as workers thought at the time. Most important to our work is the crystal structure of 3dLW that they find. Although 3dLW has low symmetry, the crystal structure is close to a body centered cubic (BCC) lattice. The BCC ordering of the molecules imposes molecular orientational order on the constitutive atoms in the lattice. This leads to cubatic orientational order, where molecular orientations are either parallel or perpendicular to each other. Since one of our key findings is molecular orientational order in 2dLW, we conjecture that this 3d molecular orientational order is somehow related to the 2d molecular orientational order we report in Chapter 4.

2.3.2 The Lewis-Wahnström model in two dimensions

To study supercooled liquid dynamics in 2d, we use a two-dimensional version of the Lewis-Wahnström model (referred to as 2dLW, see Figure 2.1). While the three-site 2dLW model does not capture the complexity of orthoterphenyl's three phenyl rings, it is sufficient to model an awkward-shaped molecule that frustrates crystal formation. The glassforming ability of 3dLW (drawn in 2d in Figure 2.1) comes from its molecular geometry as approximating an isosceles triangle with 75° apical angle. The 75° angle is a geometrical frustration that inhibits crystal formation, as the molecules do not fit together in a way conducive to translational patterns. Our other option was to study what is called a binary glass, a two-component glassforming system. In three dimensions, both one-component molecular systems and binary systems are studied in the context of supercooled liquids. In two dimensions, however, binary and polydisperse systems dominate the literature due to the difficulty of supercooling one-component molecular liquids. We chose to design a one-component su-

percooled liquid because 2d studies exclusively examine binary glasses with few exceptions. With Flenner and Szamel's conclusions about fundamental differences of dynamics of binary glasses in 2d and 3d, we were very hesitant to study binary systems since our ultimate goal is to understand dynamics in general. [9] Part of our findings in this thesis is that our 2dLW model overcomes this difficulty and readily supercools in two dimensions, complete with dynamical features seen in 3d systems.

2.4 Simulation parameters

Our simulations were carried out in the microcanonical (NVE) ensemble with square periodic boundary conditions. The equations of motion were numerically integrated using the Velocity Verlet algorithm. Rotation was handled using RATTLE, a constraint dynamics algorithm designed to work with Velocity Verlet.[23] We used RATTLE to fix bond-length constraints for the three atoms in each molecule, enforcing rigidity at every integration step. RATTLE fixed a 1σ bond-length constraint between the center atom and either outer atom. To fix the apical angle, a phantom bond of length $2\sin((75/2)^\circ)$ was enforced between the outer atoms. The RATTLE tolerance was set to 10^{-7}. Our time step was $\delta t = 0.001\tau$.

The 2dLW molecules are bent-core trimers consisting of three rigidly bound atoms represented by three Lennard-Jones sites with bond length σ and 75° apical angle (see Figure 2.1). Each Lennard-Jones site interacts with all other Lennard-Jones sites in the system except for the other two sites in the same molecule.

We used a shifted, truncated, three-site Lennard-Jones pair potential given by Equation 2.4. The Hamiltonian for our model is identical to that of the Lewis-Wahnström model,

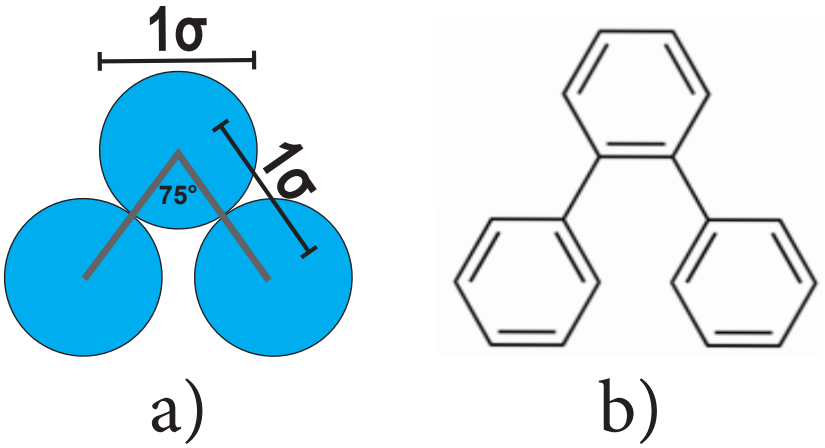

Figure 2.1: (a) A two-dimensional version of the Lewis-Wahnström model for ortho-terphenyl. (b) Chemical structure of ortho-terphenyl projected onto two dimensions.

except we are conducting our study in two spatial dimensions rather than three.

$$V(\mathbf{R}) = \sum_{\substack{j,k \\ j<k}}^{N} \sum_{a,b=1}^{3} u(r_{ja,kb}), \qquad r_{ja,kb} = |\mathbf{r}_{kb} - \mathbf{r}_{ja}| \tag{2.4a}$$

$$u(r) = \begin{cases} u_{LJ}(r) - u_{LJ}(r_c) & r \leq r_c \\ 0 & r > r_c \end{cases} \tag{2.4b}$$

$$u_{LJ}(r) = 4\epsilon[(\sigma/r)^{12} - (\sigma/r)^6] \tag{2.4c}$$

The cutoff distance is $r_c = 2.5\sigma$ by convention. V is the total potential energy of the system, and r_{ab} is the distance between two atoms labelled a and b.

Like the usual Lennard-Jones potential, ϵ is the potential well depth, and m and σ are the mass and diameter of a site, respectively. We use Lewis and Wahnström's choice of physical units, where $\sigma = 4.83$ Angstroms and $\epsilon/k_B = 600K$. Dimensionless time is given in units of t/τ, where $\tau = \sqrt{m\sigma^2/\epsilon}$. We let $m = 77$ amu, so $\tau \approx 2$ picoseconds. We also define temperature as a function of average kinetic energy, since we are in the constant NVE

ensemble where temperature fluctuates. Instantaneous temperature is given by equipartition:

$$k_B T = \frac{2\mathcal{K}}{3N} \tag{2.5}$$

where $\mathcal{K}$ is the system kinetic energy, and N is the number of molecules in the system. While T fluctuates, the ensemble average $\langle T \rangle$ does not - whenever temperature is mentioned in the report, we mean $\langle T \rangle$.

2.5 Protocols

Computer simulations like ours are sometimes referred to as computer experiments, since the aim of the simulation is to produce data about some system. This is in close analogy to taking a measurement in a laboratory setting. Like with real experiments, a detailed write-up of the method is crucial for good science. Readers may be interested in studying our model, or wish to use our methods to study their own. It may be that we or others need to reproduce our results. In any case, we present details of the important protocols programmed into our simulation.

2.5.1 Beginning the simulation

We begin the simulation by specifying an initial configuration file consisting of positions for each atom. For simplicity, we begin with a crystal (square) lattice configuration (see Figure 2.2). There are many ways to assign initial configurations, but it requires little code to produce a repeating pattern like a crystal structure. This initial lattice configuration also avoids overlap events of soft-spheres that lead to numerical instability.

Next, we assign an initial velocity distribution to the atoms in the lattice. The velocities are obtained using random numbers picked from a normal distribution with zero mean and unit variance, and scaling by the square root of a desired initial temperature (in units of $k_B T/\epsilon$). This ensures that the system's center of mass momentum $\mathbf{P}_{CM}$ is near zero. To

zero the center of mass momentum within numerical precision, a simple routine subtracted each component of the vector $\mathbf{P}_{CM}/3N$ from the momentum vector of each atom.

Our model system consists of rigid bodies, so it is also desirable to zero the initial angular momentum of the system. From classical mechanics we have the relation $\boldsymbol{L} = \overleftrightarrow{\boldsymbol{I}} \cdot \boldsymbol{\omega}$, where $\boldsymbol{L}$ is the system angular momentum, $\overleftrightarrow{\boldsymbol{I}}$ is the inertia tensor of the system of particles, and $\boldsymbol{\omega}$ is the system angular momentum all with respect to the origin at the center of the box. Projecting the 2-dimensional system onto the z = 0 plane in 3-D Cartesian coordinates, note

$$\boldsymbol{L} = \overleftrightarrow{\boldsymbol{I}} \cdot \boldsymbol{\omega} = \begin{bmatrix} I_{11} & I_{12} & 0 \\ I_{21} & I_{22} & 0 \\ 0 & 0 & I_{33} \end{bmatrix} \cdot \begin{bmatrix} 0 \\ 0 \\ \omega_z \end{bmatrix} = \begin{bmatrix} 0 \\ 0 \\ I_{33}\omega_z \end{bmatrix}$$

It is simple to calculate I_{33} and $\boldsymbol{L}$:

$$I_{33} = \sum_{\alpha} m_\alpha (x_{\alpha,1}^2 + x_{\alpha,2}^2)$$

$$\boldsymbol{L} = \boldsymbol{R}_{cm} \times \boldsymbol{P}_{cm} + \sum_{\alpha} (\boldsymbol{r}_\alpha \times \boldsymbol{p}_\alpha)$$

where α denotes indexing over all the particles and $x_{\alpha,1}, x_{\alpha,2}$ indicates the separation of the particle from the origin in the two Cartesian coordinates.

Angular momentum is finally removed by subtracting from each atom's velocity the cross product of $\boldsymbol{\omega}$ and the position vector of the atom. Note that by the definition of $\boldsymbol{L}$, the angular momentum will not be a conserved quantity due to periodic boundary conditions.

2.5.2 Simulated Annealing

Our initial configuration is a lattice, but we aim to study a liquid. The next step is to melt the lattice to obtain liquid configurations. We do this through a process called simulated annealing. The idea is to use an initial velocity distribution scaled to a high temperature ($k_B T/\epsilon = 5.0$ is more than sufficient), and wait for the lattice to melt. We recalculate the

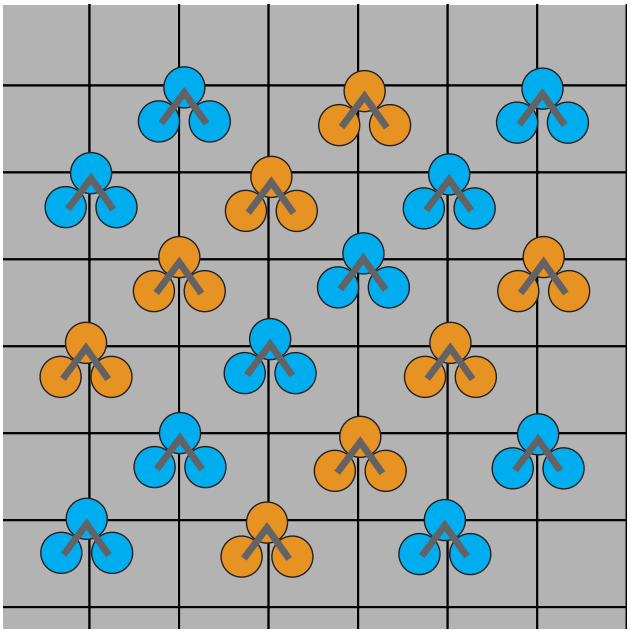

Figure 2.2: An example of a square lattice configuration used for initialization. The lattice configuration was generated using a series of tiles each with a molecule on the top right and bottom left corner of a tile. The molecules are identical. The process begins by choosing an origin (a blue tile) and populating the adjacent north, south, east, and west with an orange tile. The orange tiles are to be surrounded by blue tiles, and so forth.

temperature, rescale particle velocities to reduce the kinetic energy, then wait 100τ before recalculating the temperature again. This process is repeated iteratively until the desired temperature is reached. 100τ is a very cautious wait period that is two orders of magnitude larger than an ordinary liquid's relaxation time. When we handle the supercooled liquids, we wait 1000τ after the last velocity rescaling before recording data. Our choice of a 1000τ is chosen to be a time by which the mean square displacement of the deeply supercooled liquid ($T^* \approx 0.35$) has hit its diffusive regime in Figure 1.2. This ensures that the liquids are given a chance to relax. Once the system has become glass, we abandon any hope of relaxing on a realistic timescale. The long waiting time 1000τ is chosen independent of temperature because we calculated time correlation functions up to $10^4 or 10^5\tau$, so waiting 1000τ was not relatively computationally costly.

An additional routine we add to simulated annealing is a packing (density scaling) routine that reduces the box size iteratively much like the cooling routine described above. Density

is an important thermodynamic variable for simulations. In the microcanonical ensemble, density is constant. Ideally, one can place the tiles for the initial lattice configuration such that the system has the desired density. We found that as the initial density $\rho\sigma^2$ approached $\rho_{CP}\sigma^2$, where $\rho_{CP}\sigma^2$ is the density at close packing, RATTLE failed to converge. This was due to severe overlapping of soft-spheres when laying down tiles, resulting in very large forces for which RATTLE was unable to 'shake' the atoms into place to satisfy the constraints.

Our solution was to begin with a low density such that the initial lattice had no overlapping molecules, then slowly increase the density. Density is related to the box length:

$$\rho\sigma^2 = \frac{N\sigma^2}{L^2} \tag{2.6}$$

where $\rho\sigma^2$ is the density, and L is the length of the box. We did not want to increase N, so the approach was to slowly shrink L during the initial steps of the simulation. The density scaling algorithm repeatedly scales all distances (and the box length) by some constant factor, while allowing the system to evolve between successive distance scalings. Shrinking distances caused overlapping, but repeatedly shrinking the distances by a small amount (1%) over a period of time was sufficiently adiabatic for RATTLE to converge. Note that this algorithm also shrinks interatomic spacings inside the molecules - however, RATTLE immediately shakes the constituent atoms back to the proper interatomic spacings.

2.5.3 Equilibrating and taking data

Applying the given routines will generate a liquid of desired temperature and density in the NVE ensemble. Ordinary liquids benefit from fast relaxation processes, with relaxation time on the order of τ. We find that our relaxation times diverge as the liquid goes from supercooled to glass. An intuitive way to understand systems with long relaxation times is to describe them as having "memory". A gas has no memory: particles collide, but are otherwise approximately non-interacting and uncorrelated. Condensed matter like liquids

and solids have memory. A liquid configuration at time 0 will look very similar to a liquid configuration at time 0.1τ, but very dissimilar to a liquid configuration at time 10τ. Statistical independence of configurations is time-dependent.

Having introduced the idea of memory, we can now describe the need to equilibrate the liquid. Since we are cooling the liquid by rescaling its kinetic energy, we push the system away from equilibrium. After a cooling event, the energy balance between kinetic and potential energies is disrupted. Classical mechanics will work to restore thermal balance between the degrees of freedom, but this is not an instantaneous process. This is the reason that we measure relaxation times and wait up to 1000τ in the supercooled liquid. Our goal is to have a range of temperatures over which the system is supercooled. This requires the careful equilibration process described. The system will otherwise vitrify, leaving us with glass rather than liquid.

Taking data is perhaps the simplest yet most resource-intensive aspect of simulation. The Velocity Verlet equations (Equation 2.1) ensure that we have access to coordinates and momenta of all particles at all times. From this information we calculate all desired observables. There are two ways to use the coordinates and momenta, of which I have employed both. The first is to record the coordinates (and/or momenta) at each timestep of the simulation onto a file for later analysis. This allows one to more easily refactor code, saves time when debugging, and allows one to backtrack and compute any number of desired observables without having to rerun simulations. The drawback is that trajectory files are massive (I have some as large as 60 GB when compressed) and one generally wants thousands of them. A simpler method is to simply compute observables while the trajectories are held in virtual memory, i.e. during the course of the simulation. We use both methods, but generally prefer the latter.

2.5.4 Taking averages

Quantitative results from simulations are reported as averages, either over time or over particles in the system - usually both. One of the challenges of studying glassy dynamics is that the characteristic slow dynamics incur very long simulation trajectories. A routine calculation for ordinary liquid simulations may become prohibitively difficult in simulations of supercooled liquids. For example, consider the mean square displacement in Figure 1.2. To capture the full range of microscopic behaviors, it was necessary to compute translational correlations over six orders of magnitude in time. While the molecular dynamics algorithm has complexity $\mathcal{O}(N^2)$ where N is the number of particles and scales linearly with time, correlation functions have complexity $\mathcal{O}(n^2)$ where n is the number of timesteps over which a quantity is correlated in time. Over many orders of magnitude in time, the process of calculating correlation functions actually dominates simulation time when it comes to CPU hours.

A trick we used to capture the six decades in Figure 1.2 was to "stitch" together mean square displacement curves. This is done by computing a set of correlation functions from $10^-1\tau$ to $10^3\tau$ and another set of correlation functions from $10^1\tau$ to $10^5\tau$. This saves time and memory because on a log-scale, one needs progressively lower resolution as the x-axis indices grows exponentially. So for the short-time set of correlation functions, we compute the correlation functions using a trajectory file where each configuration is separated from the next by 0.1τ. For the second set, we have the same but with a time between configurations of 10τ. We then combine the curves for a concise figure. This lets us capture all in one plot the short-time β relaxation, the long-time α relaxation, and a clear plateau separating the two.

CHAPTER 3

Supercooled dynamics

This chapter describes the nature of slow dynamics in 2dLW. First, correlation functions are introduced as a way to study time-dependent phenomenon in a statistical context. We move on to define a number of dynamical quantities and track their evolution in time for 2dLW systems at different temperatures. We show positional correlations and dynamical degrees of freedom vanish only over large distances and times, which indicates that the 2dLW systems are disordered. Finally, we present and analyze our dynamical results in light of supercooled liquid theory, and establish that our 2dLW model has a temperature range over which it is a fragile supercooled liquid. Our argument for the liquid's fragility is made precise using comparison of the temperature dependence of the diffusion constant in 2dLW to literature and theory.

There are a number of studies on 2d supercooled dynamics that we review here. Flenner and Szamel in 2015 were the impetus for the revival of 2d studies with their claims that 2d dynamics could not be compared to 3d dynamics. [9] A number of publications arose in the subsequent years demonstrating how cage-relative coordinates recover 2d glassy dynamics. [10] [11] [12] We follow these studies in using cage-relative coordinates for translational dynamical quantities like the mean square displacement. A decade earlier, Shintani and Tanaka

introduced a one component supercooled liquid model using the Lennard-Jones potential and an ad-hoc anisotropic spin parameter. [24] They are the first to design a 2d glass-forming model liquid of one-component particles, and we have not been able to find studies using other such models other than our study of 2dLW. Interestingly, Shintani and Tanaka find that the slow dynamics in their model arise from medium-range crystalline ordering in the supercooled liquid. We make a similar claim with an important distinction. Shintani and Tanaka's model has five-fold symmetry in the spin term and shares a low-energy triangular lattice configuration with the Lennard-Jones potential. For this reason, the crystalline order they find are crystal nuclei or crystallites. Our model does not have any spin terms, so our molecular orientational order is also subject to geometric constraints from which the spin terms are free. Moreover, we are unsure of the nature (or existence) of crystals of 2dLW and as such do not claim that our medium-range order has any crystalline origin.

3.1 Correlation function

A dynamical observable $A(t)$ is in general a function of positions and momenta of particles in the system of interest. Given another dynamical observable $B(t)$, we form the equilibrium time correlation function

$$C_{AB}(t', t'') = \langle A(t')B^*(t'')\rangle \tag{3.1}$$

where the brackets indicate what is called an ensemble average, and * indicates complex conjugation. [25] An ensemble average of a function is computed by taking the mean of a function using the equilibrium probability distribution of microstates. For simulation, this can be approximated by a time average over a finite subset of the ensemble. A time average is taken by averaging over phase space points at a time t' and presenting the results (assuming time translation invariance) as a function of the time interval $t" - t'$. The assumed equivalence between ensemble average and time average is justified using the ergodic hypothesis - which

notably fails in glasses. Correlation functions are often physically meaningful as the Fourier transformation of spectroscopic data. Additionally, correlation functions arise naturally in statistical contexts outside of physical science as well. For our purposes, correlation functions comprise a standardized language to quantitatively describe microscopic dynamics of supercooled liquids.

3.2 Autocorrelation and mean square displacement

To study supercooled dynamics, we consider time correlation functions involving the center-of-mass motion of the molecules, and orientation of each molecule. These correlation functions will allow us to describe the translational and rotational motions of our system.

The orientational autocorrelation function $C_{n,s}(t)$ (see Figures 3.2, 3.1) determines how much one molecule's initial orientation is correlated with its orientation at some later time t. $C_{n,s}(t)$ is given by

$$C_{n,s}(t) = \left\langle \frac{1}{N} \sum_{j=1}^{N} T_n(\hat{\mathbf{\Omega}}_j(0) \cdot \hat{\mathbf{\Omega}}_j(t)) \right\rangle \tag{3.2}$$

$$\hat{\mathbf{\Omega}}_j(t) \cdot \hat{\mathbf{\Omega}}_j(0) = \cos(\theta_j(t))$$

where T_n is the nth Chebyshev polynomial of the first kind, N is the number of molecules, $\hat{\mathbf{\Omega}}_j(t)$ is the unit orientation vector of molecule j, and the angle brackets denote an average over configurations. $C_{n,s}(t)$ is written such that if the orientation of molecule j becomes uncorrelated with itself over time, $C(t)$ will decay to 0 over time. The s denotes that the quantity is a single-molecule (autocorrelational) property. These Chebyshev polynomials have the property:

$$T_n(cos\theta) = cos(n\theta)$$

which is sufficient to define our autocorrelation function, as the dot product between unit

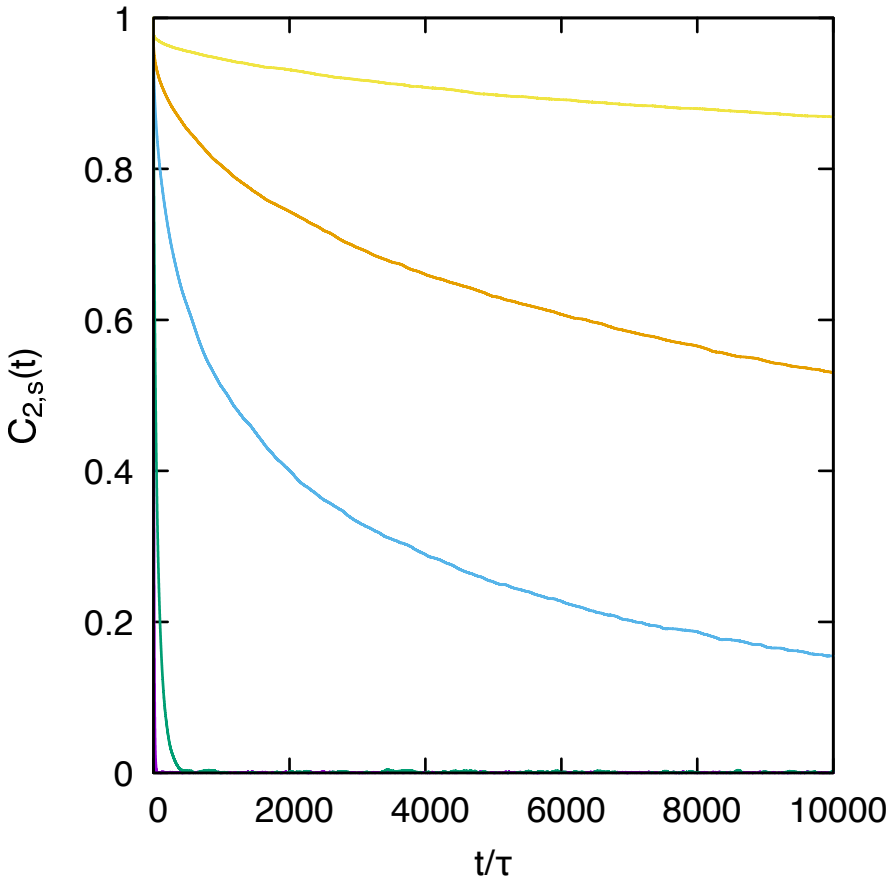

Figure 3.1: The orientational autocorrelation function $C_{2,s}$ for the N = 800 2dLW systems at different temperatures. The temperatures and colors correspond to those in Figure 3.2

.

orientation vectors is a cosine. The choice of n in T_n is related to the symmetry of the angular information we are interested in. For nematic systems, we would use T_2, and for our molecular hexatic system we use T_6. In Figure 3.1, we looked for nematic order using T_2. We found that there was no correlation at long times in all of the 2dLW liquids. We contrast this with T_6 in Figure 3.2, where there is evidently finite long-time order with a degree of symmetry we would not have even guessed was there. Note that in three dimensions, the autocorrelation function is defined using Legendre polynomials in $cos\theta$ rather than Chebyshev polynomials.

For translational dynamics, we instead focus on the mean square displacement $\Delta r^2(t)$ (Equation 1.7, 1.9). Though mean square displacement is not stricly a correlation function, its time derivative is related to the position-velocity correlation function, and the mean

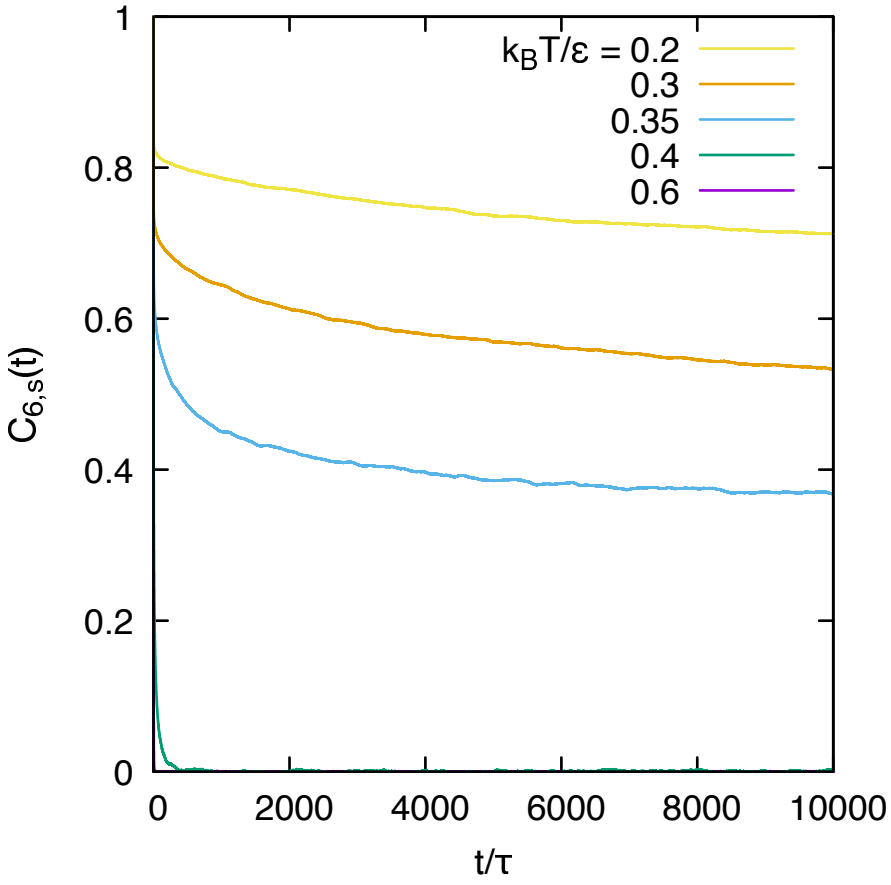

Figure 3.2: The orientational autocorrelation function $C_{6,s}$ for the N = 800 2dLW systems at different temperatures. Curves are averages over 10^5 trajectories.

square displacement calculated in much the same way as correlation functions. There is also a density-density time correlation function called the van Hove function, and we compute its Fourier transform in the form of the self-part of the intermediate scattering function (Equation 3.3). [25] The self-intermediate scattering function is given by:

$$F_s(q,t) = \left\langle \frac{1}{N} \sum_{j=1}^{N} e^{i\boldsymbol{q}\cdot(\boldsymbol{r_j}(t)-\boldsymbol{r_j}(0))} \right\rangle \tag{3.3}$$

where q is a wavevector chosen to be the first sharp peak of the static structure factor. However, we find that analysis of the mean square displacement is sufficient to study translational autocorrelation.

Mean square displacement gives valuable information about the dynamics because of its clear physical meaning. Its utility has made it convention to focus attention on the mean square displacement in favor of other simple translational correlation functions. The mean square displacement at short times is marked by a ballistic regime (β relaxation) where particles cover distances proportional to time, which shows up as a curve of slope 2 in a log-log plot of the mean square displacement versus time. The hydrodynamic regime becomes relevant when particles diffuse throughout the system according to Brownian motion. This diffusive regime (α relaxation) can be shown to appear in the log-log plot of mean square displacement versus time as a line of slope 1. When a system is deeply supercooled, α and β relaxations become separated in time by an intermediate plateau in a phenomenon called "transient localization". [7] The mean square displacement is powerful in allowing us to keep track of these three regimes.

Equally important is the simple relation between mean square displacement and the diffusion constant D. In two dimensions, D is given by

$$\frac{\partial(\Delta r^2(t))}{\partial t} = 4D \tag{3.4}$$

[25] In practice, one must select only the diffusive regime of $\Delta r^2(t)$ before taking the time

derivative. This diffusive regime is clearly indicated by the portion of $\Delta r^2(t)$ that corresponds to the line of slope 1 in the log-log plot of $\Delta r^2(t)$ versus time (refer to Figure 1.2).

3.3 Phenomenology

When we refer to the slow dynamics of supercooled liquids, we really mean to make a quantitative statement about the functional form of some dynamical quantity like the diffusion constant. Based on our results in Figure 3.3, we say that 2dLW is a fragile supercooled liquid for $T* \geq 0.35$, afer which we see a dynamical crossover to Arrhenius-type activated dynamics. Both fragility and the Arrhenius behavior are defined by the particular functional form of the diffusion constant (or quantities representing other dynamical processes). The Arrhenius equation is known to chemists as the formula governing temperature dependence of reaction rates. The Arrhenius equation is given by:

$$D = D_o e^{-B/T} \tag{3.5}$$

where D_o and B are nonnegative fitting parameters while T is temperature. The physical picture of Arrhenius dynamics is clear: D is large, i.e. a system has fast dynamics, when temperature is large. Likewise, a system has slow dynamics when temperature is low. In particular, if diffusion is Arrhenius then we expect activated processes to dominate diffusion via rare thermally driven diffusion events. B has the physical meaning of the activation energy (modulo a dimensionful factor like k_B).

Fragility describes diffusion obeying the following functional form:

$$D(T) = Ae^{-\frac{B}{T-T_o}} \tag{3.6}$$

where A, B, and T_o are parameters of the fit. This function is called the Vogel-Fulcher-Tamman (VFT) law. [7]

When a glassy system is well-described by VFT, we refer to the system as kinetically 'fragile'. [26] The idea of fragility is that diffusion processes precipitously slow down (and relaxation times spike sharply) at some nonzero temperature T_o. This is in contrast to Arrhenius dynamics which suggest that diffusion continues to slow down gradually until zero temperature. When dynamics are described well by the Arrhenius equation, we refer to the system as 'strong'. From Figure 3.3, VFT followed by an Arrhenius form is a very good fit to our diffusion constants. For this reason, we conclude the dynamics of our 2dLW system crossover from fragile to strong as the liquid undergoes supercooling and an eventual glass transition. This is consistent with molecular dynamics studies of 3dLW. [21]

We mentioned previously another important phenomenon called dynamical heterogeneity (DH). A system is dynamically heterogeneous when the microscopic dynamics vary spatially. DH is a trademark of deeply supercooled and glassy systems, where relaxation processes occur on different timescales at different locations in a sample. DH relaxations are characterized by a molecule seeing long periods of inactivity punctuated by short-lived bursts of motion. We draw displacement maps in Figure 3.5 to track DH in N=1800 2dLW. We find that on the timescale that the majority of the system is inert, small pockets of activity exist in separated regions of the system. This is evidence of DH, which is an encouraging result suggesting our 2dLW model captures another essential feature of glassy dynamics.

3.4 Amorphous solid

We have presented a great deal of dynamical information. This section is a detour to examine temperature dependence of positional correlations. We show that there is no crystal lattice in our simulations of 2dLW. Since the dynamics arrest (time correlation functions have no noticeable decay over $10^5\tau$) while particle positions remain amorphous, we conclude that our 2dLW system at low temperatures ($T^* < 0.35$) becomes glass. This was also strongly indicated by the dynamical crossover in Figure 3.3 where diffusion becomes best described by

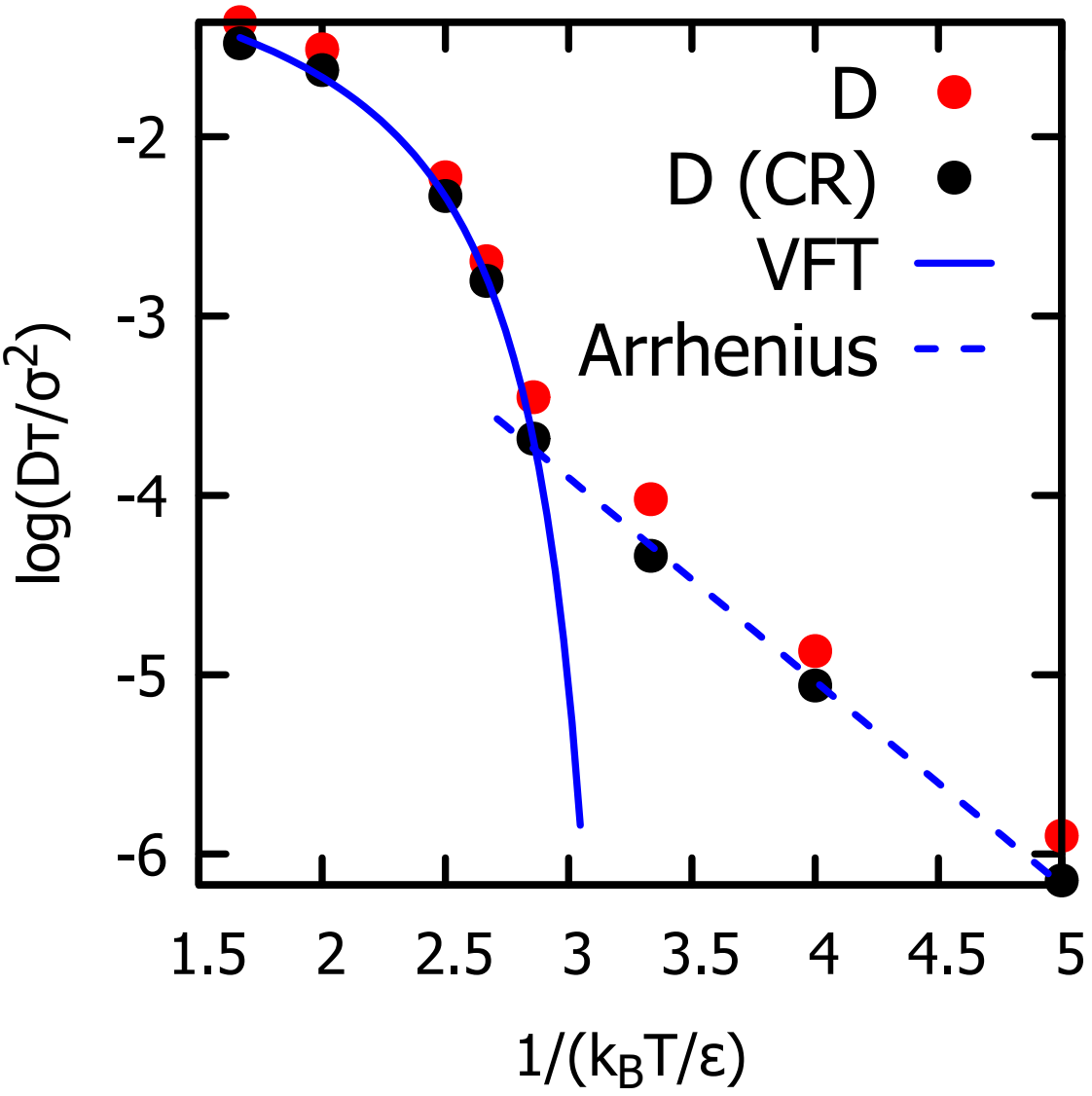

Figure 3.3: Temperature dependence of the cage-relative self-diffusion constant (CR-D) and ordinary self-diffusion constant (D) for N=800 2dLW systems. The solid line is a fixed T_o VFT law through the liquid and supercooled liquid temperatures for CR-D. The dashed line is an Arrhenius equation fit to CR-D for the temperatures at which 2dLW is glass. The figure plots logarithm of diffusion versus inverse temperature to emphasize the Arrhenius-type dynamics at low temperatures. VFT indicates the following function: -1.007161 - 0.131572/(T-0.300949). Arrhenius indicates: -0.495461 - 1.135303/T. Diffusion constants are computed using long-time behavior ($t > 80000\tau$) of the cage-relative mean square displacements. Each data point corresponds to diffusion constants computed from 2×10^6 trajectories.

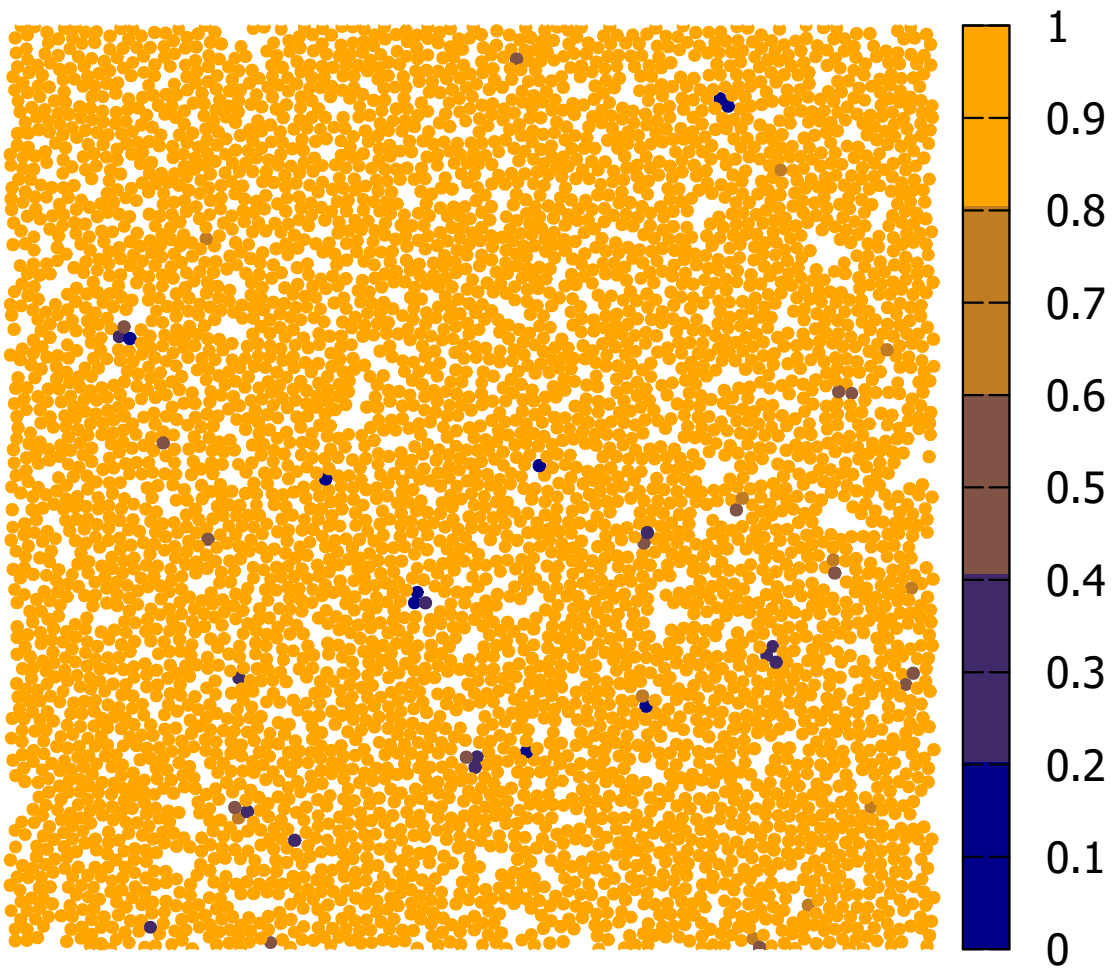

Figure 3.4: Displacement map for the N=1800 ordinary liquid 2dLW, T* = 0.65. Colors are assigned according to the displacement of the molecule (measured in σ) after 10,000τ.

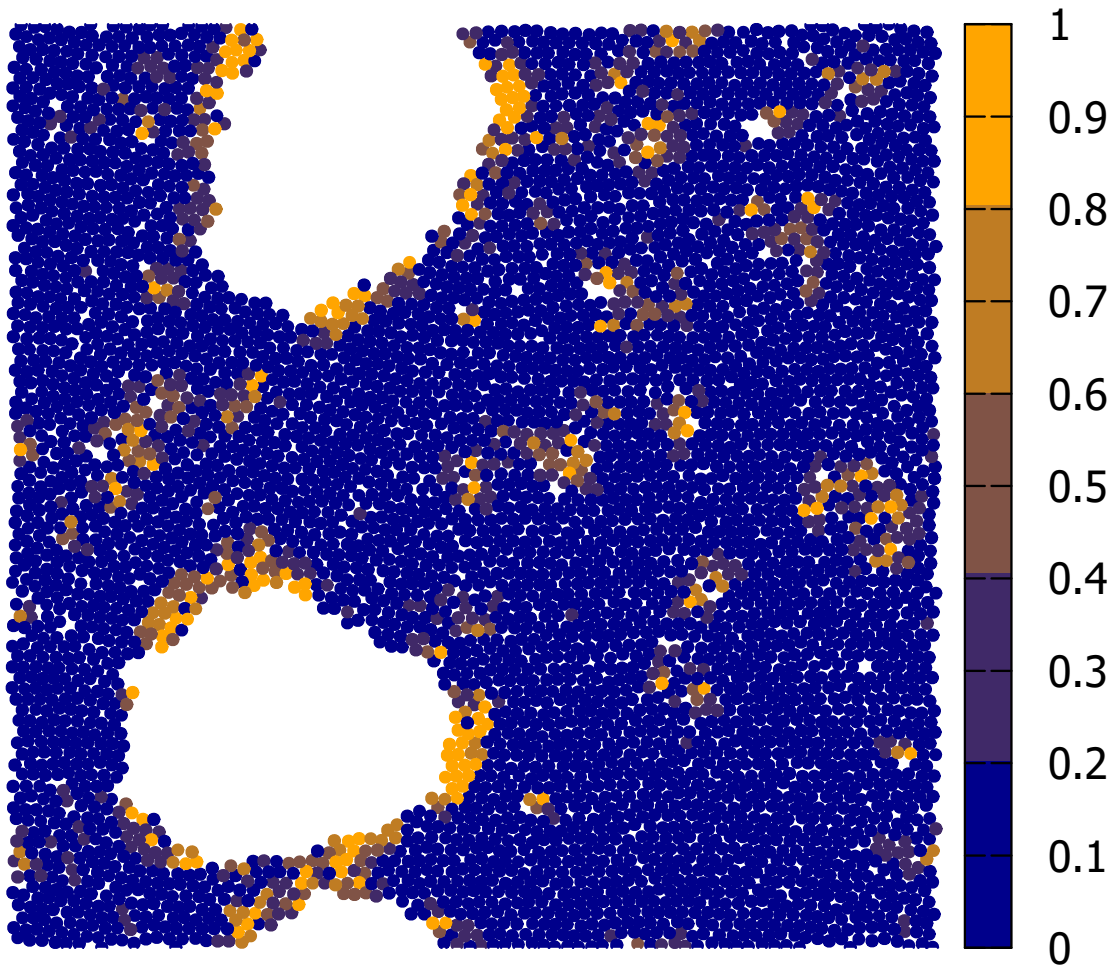

Figure 3.5: Displacement map for the N=1800 supercooled liquid 2dLW, T* = 0.35. Colors are assigned according to the displacement of the molecule (measured in σ) after 10,000τ. The voids are a known phenomenon resulting from "cavitation", discussed in Section 4.4.1.

Arrhenius. The absence of long-range translational order at any temperature confirms that we never encounter 2dLW crystals. Then between the high temperature liquid and the glass, we must have a supercooled regime. The temperature ranges for the different behaviors of 2dLW given in the "Phase Diagram" section of Chapter 1 are determined using a combination of the temperature dependence of the diffusion constant, the divergence of relaxation times with temperature, and the (absence of) translational structure as determined by positional correlation functions.

The primary correlation function we use to measure positional correlations is called the radial distribution function, $g_2(r)$. The radial distribution function measures how local density changes with distance from a reference particle. Intuitively, $g_2(r)$ is proportional the conditional probability of finding a particle at a distance r given that there is also a particle at the origin. We computed $g_2(r)$ for a secondary model consisting of a bent-core trimer comprising an equilateral triangle molecule with an obvious triangular lattice ground state. $g_2(r)$ for this system is representative of what the radial distribution function looks like for a 2D crystal (see Figure 3.6). This should be compared with Figure 3.7, which computes $g_2(r)$ for the 2dLW systems. For the crystal-forming system in Figure 3.6, there is a stark contrast between the top (coldest) curve and the bottom curves. This difference is attributed to a first-order phase transition from liquid to crystal. For our glass-forming 2dLW system in Figure 3.7, there is no clear structural change as temperature is lowered through supercooled liquid to glass. It is not pictured in Figure 3.7, but $g_2(r)$ at $T^*=0.4$ is indistinguishable from $g_2(r)$ at any higher temperatures. We conclude that there is no crystal structure in our 2dLW simulations.

The radial distribution function is given formally as an ensemble average over pairs:

$$g_2(\mathbf{r}) = \frac{1}{N\rho}\left\langle \sum_j^N \sum_{k\neq j}^N \delta(\mathbf{r} - \mathbf{r_{jk}}) \right\rangle \tag{3.7}$$

$$= \frac{V}{N^2}\left\langle \sum_j^N \sum_{k\neq j}^N \delta(\mathbf{r} - \mathbf{r_{jk}}) \right\rangle \tag{3.8}$$

where δ is the Dirac delta function, V is the volume of the space we are considering, and r_{jk} indicates the separation vector between molecules j and k.

In practice, we calculate $g_2(r)$ by assuming a homogeneous and isotropic liquid, so we can make the following simplification:

$$g_2(r) = \begin{cases} \frac{1}{N}\frac{1}{4\pi r^2 \rho}\left\langle \sum_j^N \sum_{k\neq j}^N \delta(r - r_{jk}) \right\rangle & \text{three dimensions} \\ \frac{1}{N}\frac{1}{2\pi r \rho}\left\langle \sum_j^N \sum_{k\neq j}^N \delta(r - r_{jk}) \right\rangle & \text{two dimensions} \end{cases} \tag{3.9}$$

We can corroborate the lack of crystal structure by computing what is called the static structure factor $\hat{S}(k)$. As $\hat{S}(k)$ is related to the Fourier transform of $g_2(r) - 1$, $\hat{S}(k)$ picks up on any periodicity in translational order - useful for finding lattice constants of a crystal, or short-range structure in a liquid. We compute the static structure factor (Figure 3.8) to rule out crystalline translational order and to find conventional scattering momenta for other scattering functions like Equation 3.3. Figure 3.8 lacks sharp diffraction peaks, and the diffuse peaks are consistent with typical liquid structure factors. From $\hat{S}(k)$ (Figure 3.8), we confirm that there is no translational symmetry in our 2dLW systems.

The static structure factor is formally given by

$$\hat{S}(k) = \frac{1}{N}\left\langle \sum_{j,k=1}^N e^{-i\mathbf{k}\cdot(\mathbf{r_j} - \mathbf{r_k})} \right\rangle \tag{3.10}$$

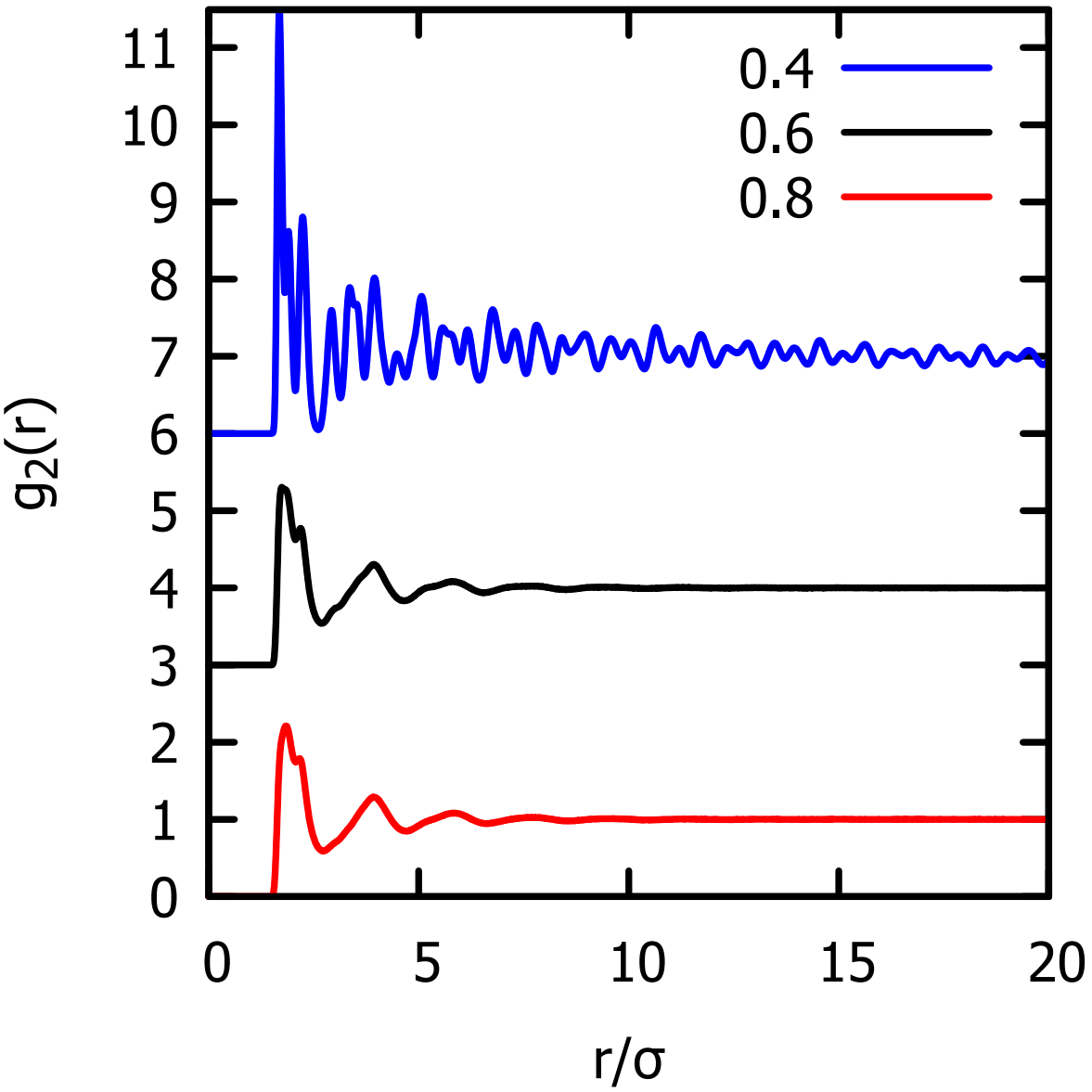

Figure 3.6: Radial distribution function of N=800 equilateral trimer (not 2dLW!) systems with 60° apical angle at different temperatures. Averages are taken over 3×10^5 configurations. The distance r is measured between the centers of mass of the molecules.

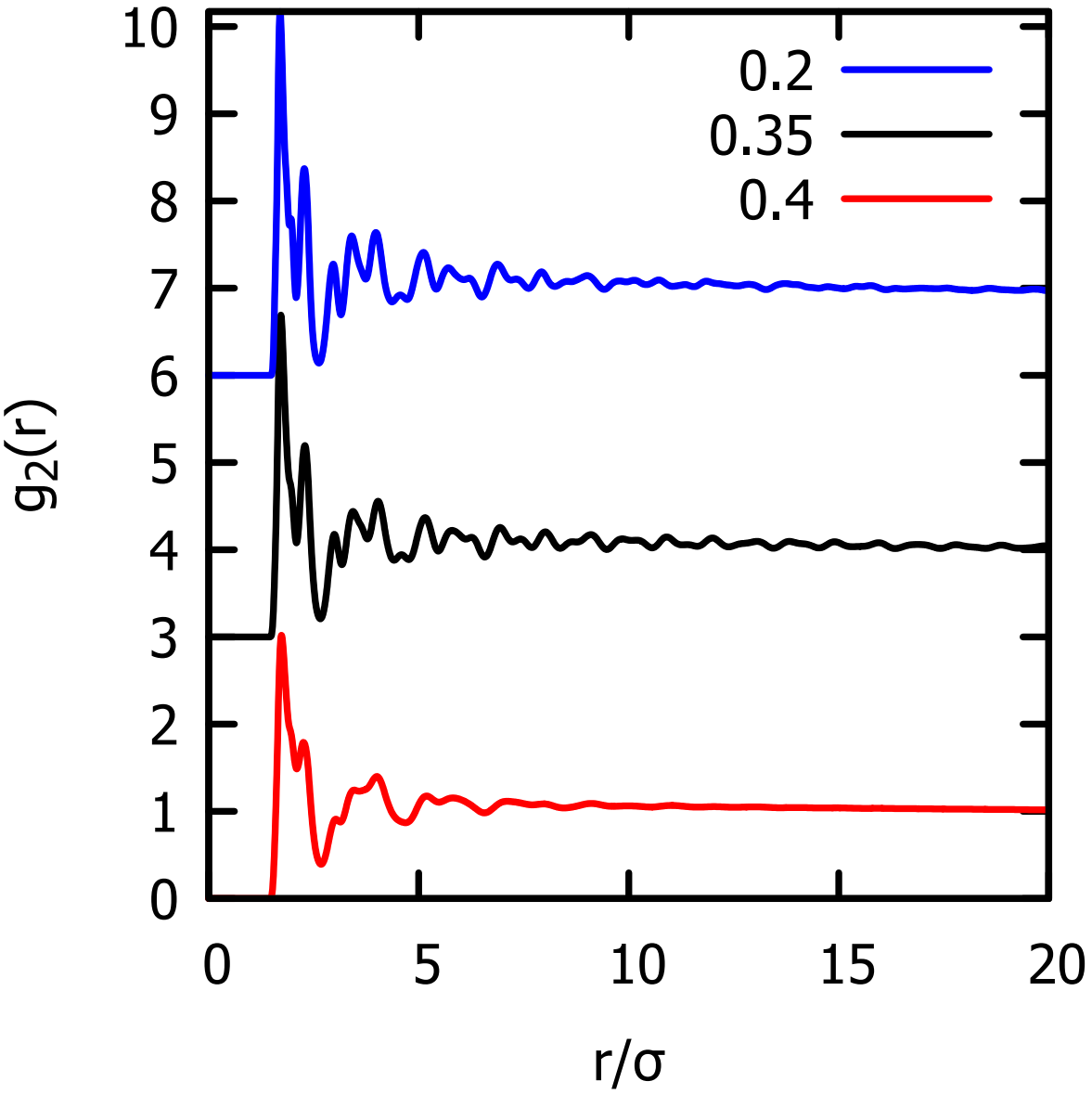

Figure 3.7: Radial distribution function of the N=1800 2dLW systems at different temperatures. Averages are taken over 3×10^5 configurations. The distance r is measured between the centers of mass of the molecules.

But in practice, we compute $\hat{S}(k)$ in liquids by relating to $g_2(r)$:

$$\hat{S}(k) = 1 + \rho \int e^{-i\mathbf{k}\cdot\mathbf{r}}(g_2(r) - 1)d\mathbf{r} + \mathrm{N}\delta_{\mathrm{k},0}$$

In two dimensions, it is given by

$$\begin{aligned}
\hat{S}(k) &= 1 + \rho \int e^{-i\mathbf{k}\cdot\mathbf{r}}(g_2(r) - 1)d\mathbf{r} + \mathrm{N}\delta_{\mathrm{k},0} \\
&= 1 + \rho \int e^{-ikr\cos\theta}(g_2(r) - 1)rdrd\theta \\
&= 1 + \rho \int \left[\int e^{-ikr\cos\theta}d\theta \right] r(g_2(r) - 1)dr \\
&= 1 + 2\pi\rho \int_0^\infty J_o(kr)r(g_2(r) - 1)dr
\end{aligned} \tag{3.11}$$

where we let $\mathbf{k} \neq \mathbf{0}$ and J_o is a Bessel function:

$$J_n(x) = \frac{1}{2\pi} \int_{-\pi}^{\pi} e^{i(x\sin\tau - n\tau)}d\tau$$

For completion, in three dimensions the static structure factor is given by

$$\hat{S}(k) = 1 + 4\pi\rho \int_0^\infty r^2 \frac{\sin(kr)}{kr}(g_2(r) - 1)dr \tag{3.12}$$

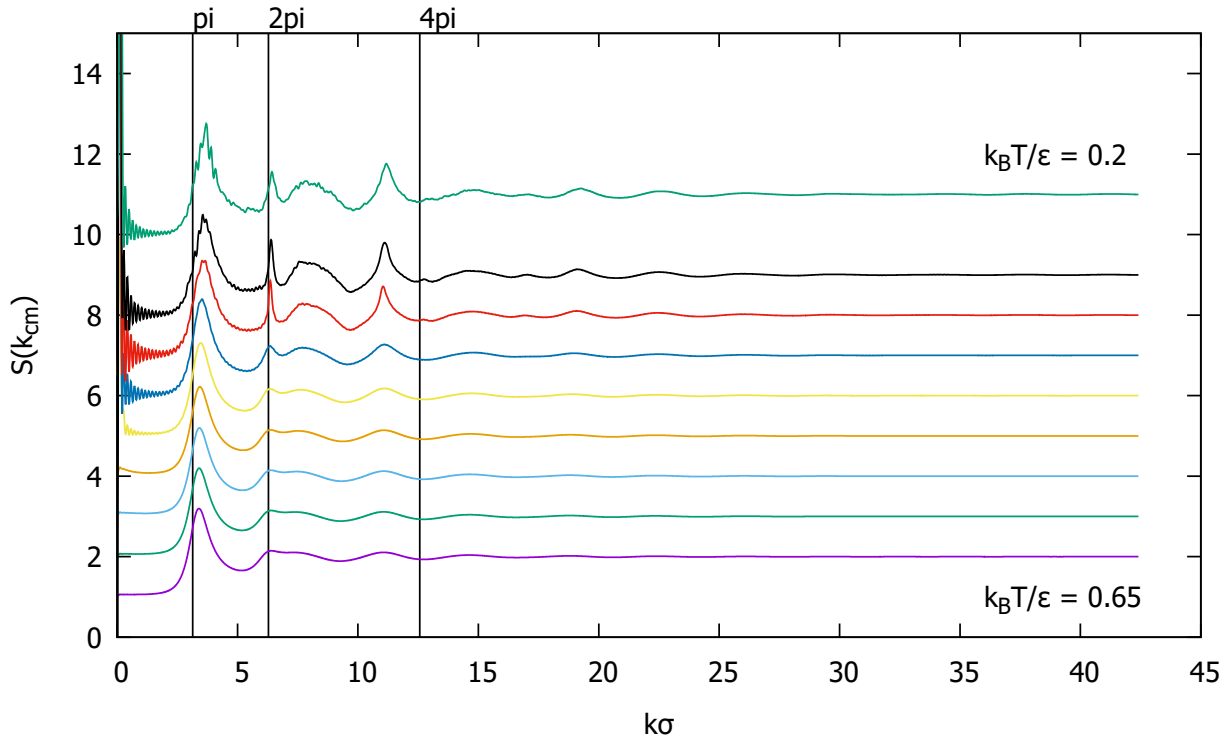

Figure 3.8: Center of mass static structure factor via Fourier transform of the pair correlation function for the system of N=1800 molecules. Averaged over 3×10^5 configurations. Temperature increases by $0.05 k_B T/\epsilon$ for each successive curve from the top. Curves are displaced vertically to improve visibility. The 2nd curve from the top ($k_B T/\epsilon = 0.25$) is missing due to corrupted data.

CHAPTER 4

Mesoscopic structure

We demonstrated that the 2dLW model systems captured the important features of supercooled dynamics. While supercooled liquids are understood to be structurally identical to ordinary liquids, we now give surprising evidence that there are in fact structural signatures of supercooling. Existing work, including the purely dynamical theories discussed in Section 2.1.1, studies dynamical phenomena in supercooled liquids as completely independent from any structural phenomena. Our results defy such literature expectations of the insignificance of structural phenomena to glassy dynamics, and as such constitute profound evidence that structural phenomena cannot be ignored in dynamical studies of supercooling. In this chapter, we elaborate on our discussion in Section 1.3 on the Fayer group's conjecture that supercooled dynamics accompany the formation of structural domains much like the pseudonematic domains in isotropic liquid crystals. [8] [27] In a similar vein, a few workers have attempted to understand fragility in the supercooled liquid as a consequence of the formation of slow, long-lived domains from locally preferred structures. [28] [29] [30] We will connect our own findings regarding mesoscopic structures in 2dLW with discussions of slow dynamics and fragility in the greater context of supercooled liquids in general.

4.1 Hexatic molecular orientational order

Close inspection of configurations of the 2dLW simulations showed that molecules' orientations would prefer lining up along six preferred axes. This is similar to order in nematic liquid crystals, in which molecules on average favor being parallel or antiparallel to a common axis called the director. In analogy to nematic liquid crystals, we refer to the six-fold molecular orientational order in the 2dLW simulations as hexatic molecular orientational (MO) order. Recall the expression for the (complex) m-fold order parameter s_m given in Equation 1.5. We gauge six-fold order using this s_6 order parameter (Figure 4.2). By construction, the magnitude of the order parameter measures the extent of order in the system on a scale between 0 and 1. A perfectly ordered system, in our case a system whose molecules line up perfectly along an axis $\hat{n}$ or the five equivalent axes generated by 60 degree rotations of $\hat{n}$, has $|s_6| = 1$. Disordered systems have lower values of the order parameter. Due to finite-size effects and thermal fluctuations, isotropic liquids will have nearly but not exactly $s_6 = 0$. In section 4.1.1, we calculate s_m for $m \neq 6$ to show that there is no significant m-adic MO order for any $m < 6$.

Consider Figure 4.2. We see that at high temperatures $T* \geq 0.45$, the order parameter is close to zero. Since we know there is no hexatic MO order in the high temperature regime, this is our baseline for a disordered system. The order parameter sees modest growth at $T* = 0.4$. We then see a drastic increase in hexatic MO order for all temperatures below this point. Given the growth of the order parameter, we conclude that there is unmistakeable structural order in the supercooled liquid ($0.35 \leq T* < 0.45$) and glass. For a discussion of how we arrived at this temperature range for the supercooled liquid, see Section 1.5. In fact, there is a hint of hexatic MO order even at $T* = 0.45$, where there is a very small but noticeable increase in order. We will elaborate on this hint in the next section. We can learn more from the order parameter by plotting its probability density, obtained by making a normalized histogram over configurations (Figure 4.3a). At high temperatures, the

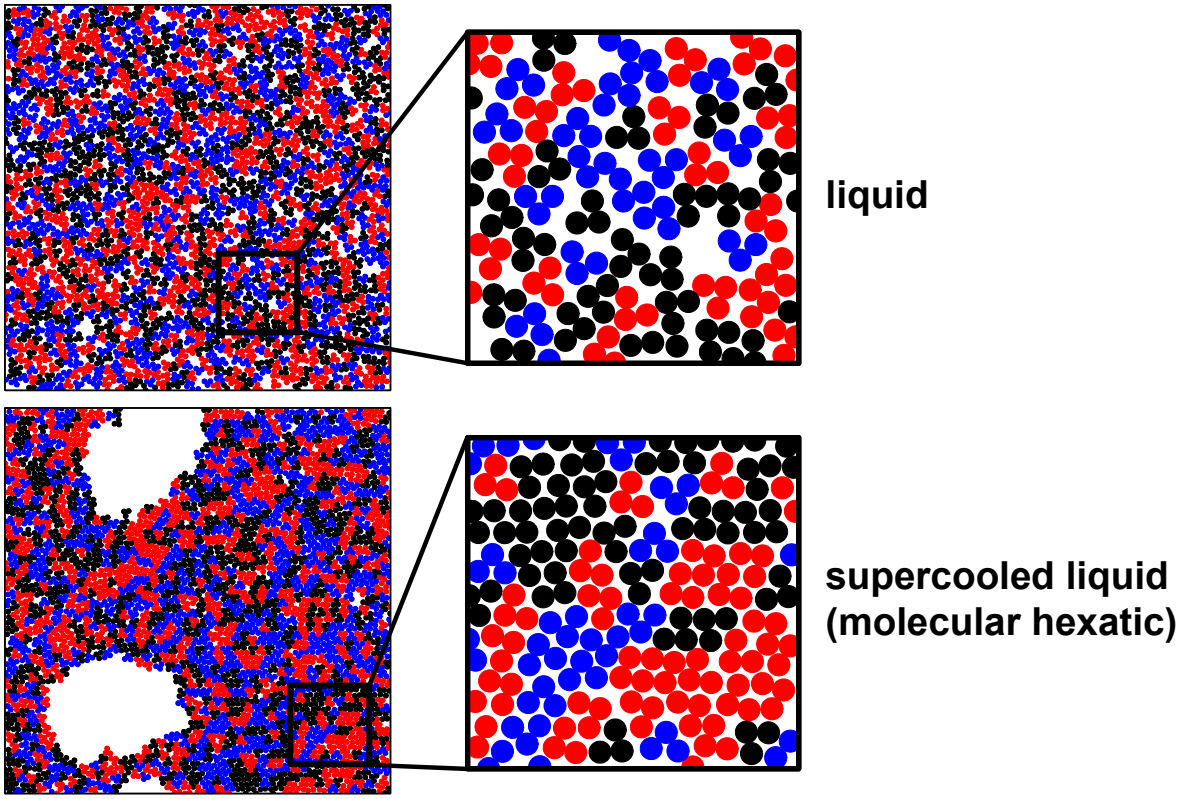

Figure 4.1: Comparison between an ordinary liquid configuration ($T^* = 0.65$) and a supercooled liquid configuration ($T^* = 0.35$), N = 1800. Molecules are assigned one of three colors depending on the angle between the molecular orientation vector and an arbitrary axis. Molecules of the same color are roughly parallel or anti-parallel to each other. The figure introduces our primary finding regarding 2dLW structure: in the supercooled liquid, structural order takes the form of six-fold molecular orientational order.

isotropic liquid's order parameter distribution is entirely consistent with finite-size effects. The order parameters in the supercooled liquid and glass are narrow with distributions peaked at significantly positive values of the order parameter. That the order parameter is even sharper in the glass, yet the magnitude of the order is much smaller than in the supercooled liquid is not a coincidence. This curious feature in the probability densities led us to examine more closely the nature of hexatic MO order in the supercooled liquid and glass. We wondered whether we had a true thermodynamic MO hexatic phase. We discuss how we arrive at the conclusion that we do not have a thermodynamic MO hexatic phase in Section 4.2. Figure 4.3 is discussed in more detail in Section 4.4.

4.1.1 How about m-adic order for m $\neq$ 6?

After learning about hexatic order, it is important to ask whether there is m-adic order for $m \neq 6$. We conducted a study at $T* = 0.65, 0.35$, and 0.2, N = 1800, of $P(s_m)$ in Figure 4.4. We only show the $T* = 0.35$ results. The result was expected: s_6 order is significant while the distributions of s_1, s_2, s_3, s_4, s_5, and s_8 do not indicate other m-adic order. In general, if m-adic order is present, we also expect $n * m$-adic order where n is any integer. The comparison in Figure 4.4 shows that the lowest m for which s_m order is significant in the supercooled liquid of 2dLW is $m = 6$. This is why we refer to the order in the supercooled liquid as "hexatic" molecular-orientational order.

4.1.2 Literature precedent

Martínez-Ratón, Díaz-De Armas, and Velasco released a study in 2018 that found packing hard objects in two dimensions can lead to molecular-orientational order with different symmetries than those found in the molecules themselves. [31] The authors find that the hexatic MO phase (what they refer to as 'triatic') is stable for hard anisotropic equilateral triangles and isosceles triangles with different aspect ratios. They use Scaled Particle Theory and a density functional theory to derive these results. Since the 2dLW model is in a sense

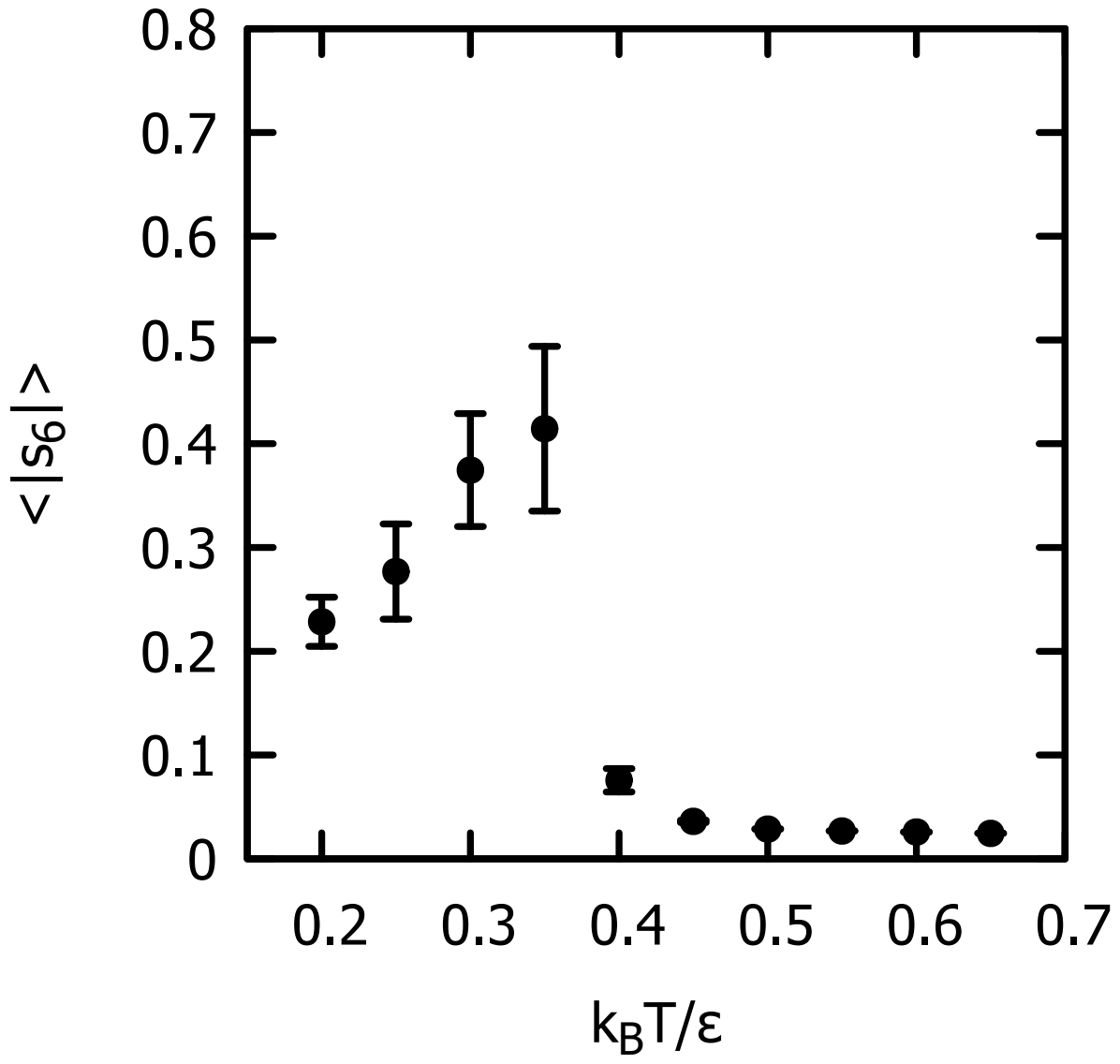

Figure 4.2: Mean of the order parameter versus temperature for the N=1800 2dLW system. Data comes from 5×10^4 trajectories. Error bars are standard error of the mean.

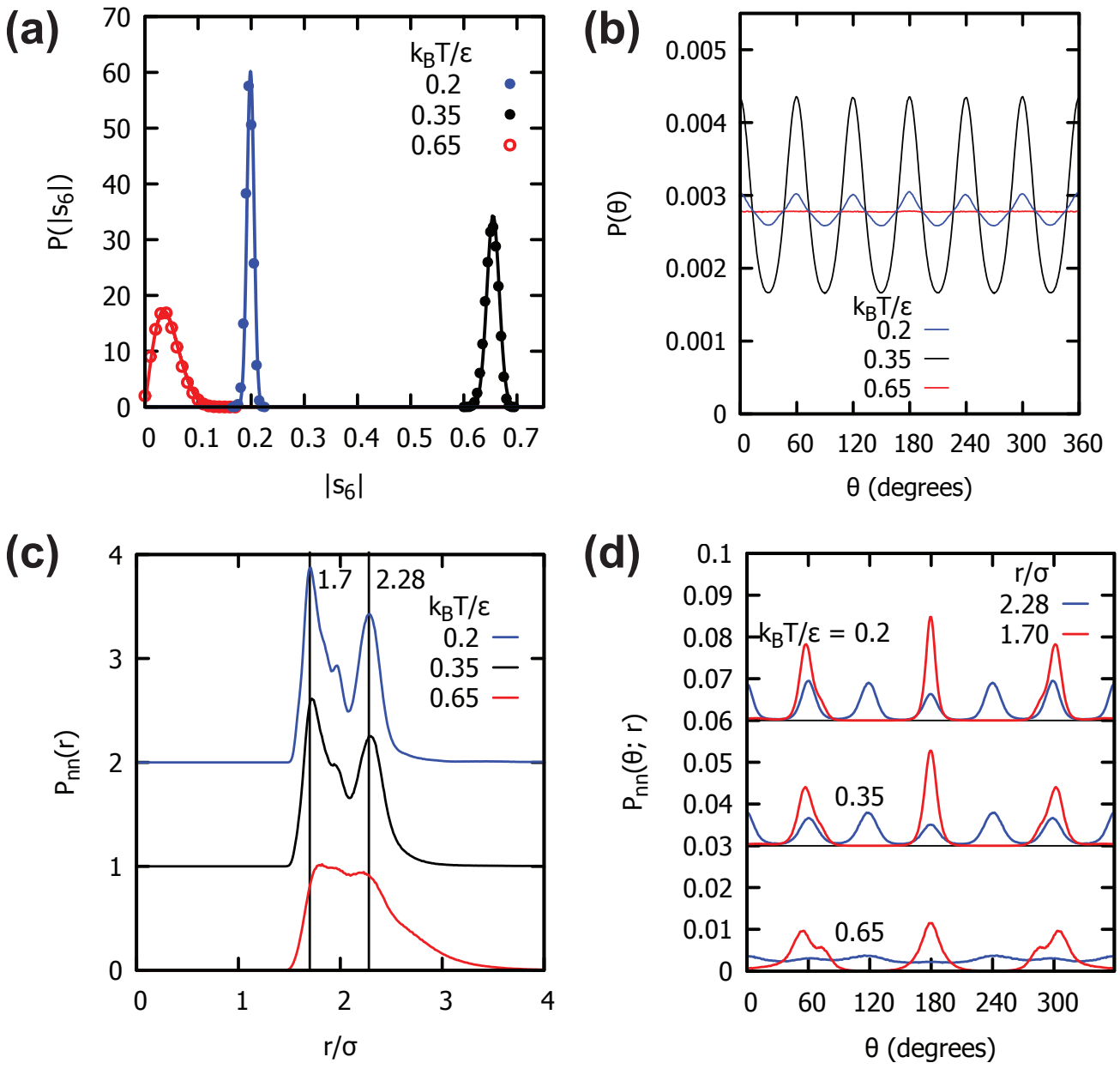

Figure 4.3: All figures correspond to systems of N=1800 2dLW molecules. (a) Probability density of the order parameter. Averages are taken over 3×10^5 configurations. Solid curves are central limit theorem predictions, but for the purposes of this thesis can be taken as guides to the eye. (b) Probability density of the relative molecular orientation angle between all pairs of molecules. (c) Probability density of the distance between Voronoi-determined nearest neighbors. (d) Probability density of the relative molecular orientation angle between neighboring pairs of molecules. (b-d) Averages are taken over 1000 configurations.

isosceles with its trimer shape, and the order they predict is the same as the kind we report, the findings of Martínez-Ratón, et. al., are very relevant to our work. There are important distinctions between our methods: their work is analytical, requiring certain assumptions and truncations to compute their answers while our numerical simulations do not require such assumptions. Further, their particles are modeled as hard isosceles triangles while ours are soft trimer molecules. The hexatic MO phase they predict also requires packing fractions larger than 0.92, which corresponds to unphysical densities in more realistic models of glass-formers. Finally, their study finds phase transitions among the differently ordered phases and as such predicts that the hexatic MO order indicates a true thermodynamic phase, unlike in our simulations. It is significant that despite the differences in model and method, we both find hexatic MO ordering. This indicates that m-adic MO ordering, $m > 2$, should be expected in models other than ours. As a preliminary study of MO ordering in different systems, we varied the apical angle in 2dLW in Appendix A. There is some evidence that some of the models we explored have MO order in the absence of a crystalline lattice, but we do not make any conclusions at this time.

4.2 Mesoscopic structure

We were able to show that we should not expect a macroscopically ordered hexatic phase of 2dLW molecules. At a qualitative level, we saw that local directors in the glass (centered on a molecule and incorporating a small box around it) were spatially heterogeneous, and local order parameters were sharply peaked around large values of the order parameter (Figures 4.6, 4.7). It is important to note that the local order parameter distributions were spatially heterogeneous, as seen by the variation in order parameter distributions in different parts of the systems in Figures 4.6 and 4.7. This indicated that upon supercooling, the liquid was forming structurally ordered domains. Our findings suggest that molecular orientational ordering leads to numerous mesoscopic structures in supercooled liquids that contribute to

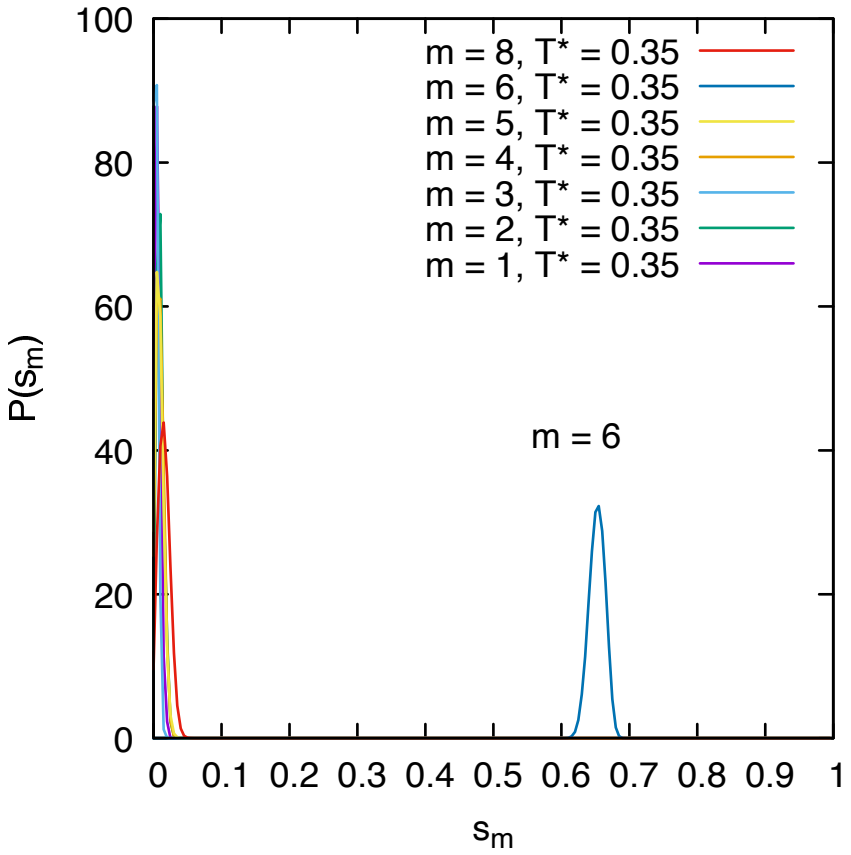

Figure 4.4: Comparison between probability distributions of s_m for a N=1800 2dLW simulation run at $T* = 0.35$. The only significant peak is for s_6.

kinetic fragility in supercooled liquids.

4.2.1 Neither macroscopic nor quasi-long-range order

Before we continue discussing structural domains, it is important to quantitatively establish that in our simulations of 2dLW molecules, the hexatic MO order is mesoscopic rather than macroscopic or quasi-long-range. To rule out macroscopic order, we plot the order parameter s_6 to test its scaling with particle number N (Figure 4.8). $< |s_6| >$ clearly vanishes (converges to zero) as $N^{-1/2}$ in the ordinary liquid and glass. $< |s_6| >$ in the supercooled liquid follows the N scaling trend of the ordinary liquid and glass. The order parameter in the supercooled liquid does not fit perfectly to $N^{-1/2}$, but it clearly vanishes at least as fast as $N^{-1/2}$. This finite-size scaling behavior rules out the possibility of macroscopic MO hexatic order (at least for the thermodynamic parameters we have chosen). Thus we conclude that the hexatic MO order we observe does not correspond to a thermodynamic phase.

Further, this shows that

$$< |s_6| > \quad \sim \quad \frac{\eta}{L}$$

where η is a correlation length and L is the length of the system. This arises from the scaling factor we determined previously, and the relation:

$$N = \rho L^2$$

From this we deduce that the convergence of the order parameter with system size is much faster than the algebraic decay (power law) predicted by Kosterlitz-Thouless-Halperin-Nelson-Young (KTHNY) theory for quasi-long-range correlations corresponding to two-dimensional liquid phases. [14] This allows us to conclude that the hexatic MO order we find is distinct from macroscopic order and KTHNY phenomenon.

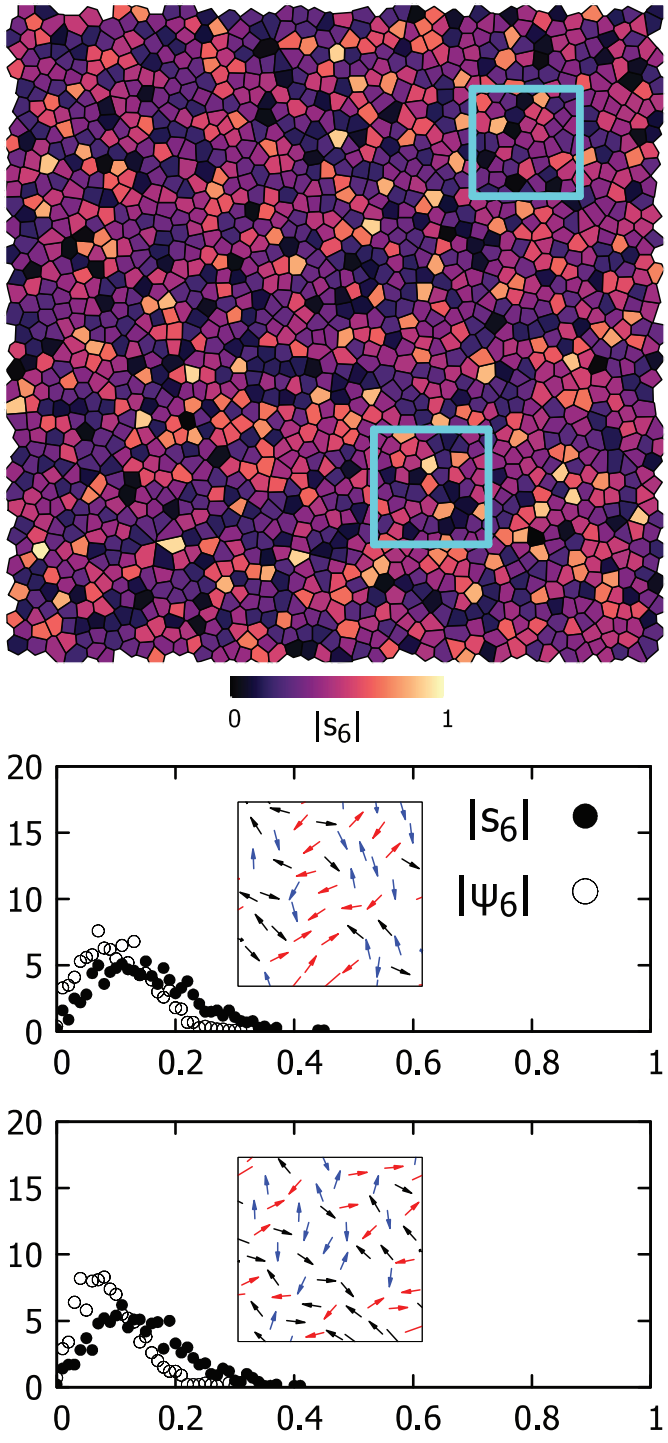

Figure 4.5: (top) Voronoi tesselation of an N=1800, T^*=0.65 system of 2dLW molecules. (bottom) Local order parameter probability density of two sections of the simulation box indicated in the top row. ψ (open circles) corresponds to bond-orientational order, and s (solid circles) corresponds to molecular-orientational order. Averages are over 1000 configurations. Inset: sections of the simulation box with molecules represented by their molecular orientation vectors, alongside the local director corresponding to that section of the simulation box.

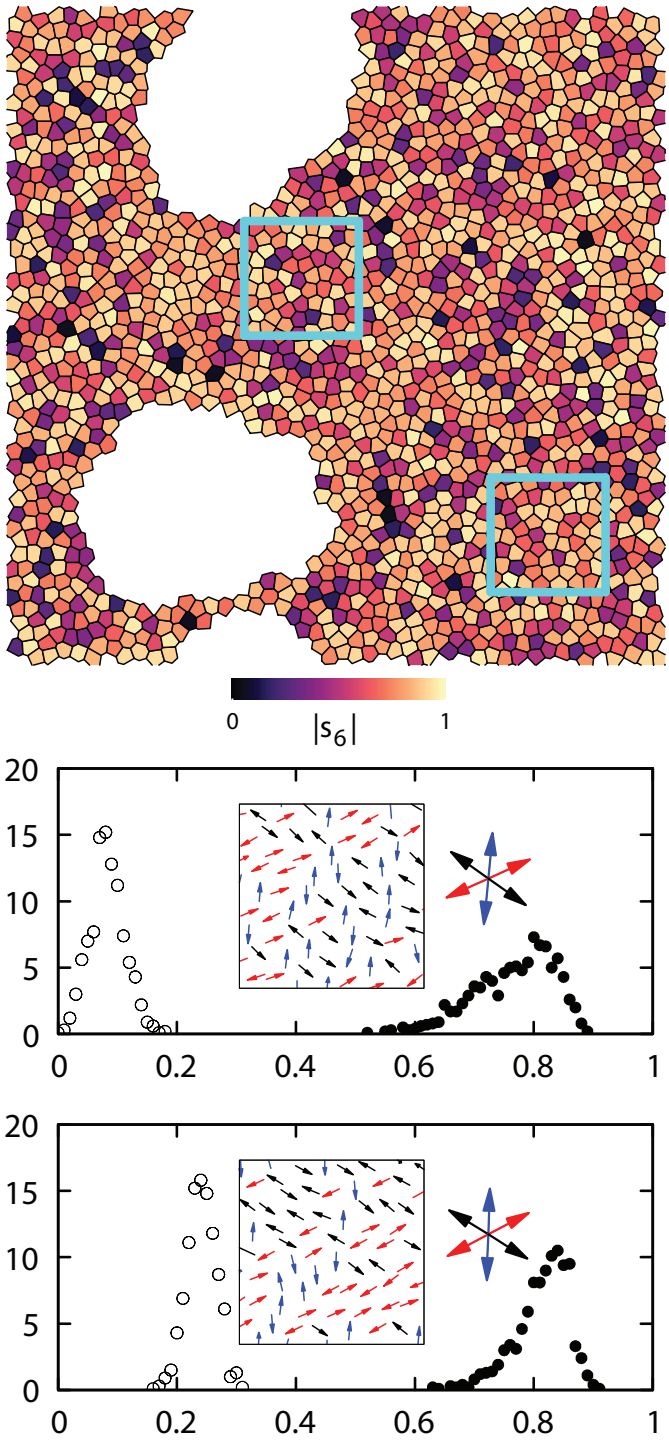

Figure 4.6: (top) Voronoi tesselation of an N=1800, T^*=0.35 system of 2dLW molecules. (bottom) Local order parameter probability density of two sections of the simulation box indicated in the top row. ψ (open circles) corresponds to bond-orientational order, and s (solid circles) corresponds to molecular-orientational order. Averages are over 1000 configurations. Inset: sections of the simulation box with molecules represented by their molecular orientation vectors, alongside the local director corresponding to that section of the simulation box.

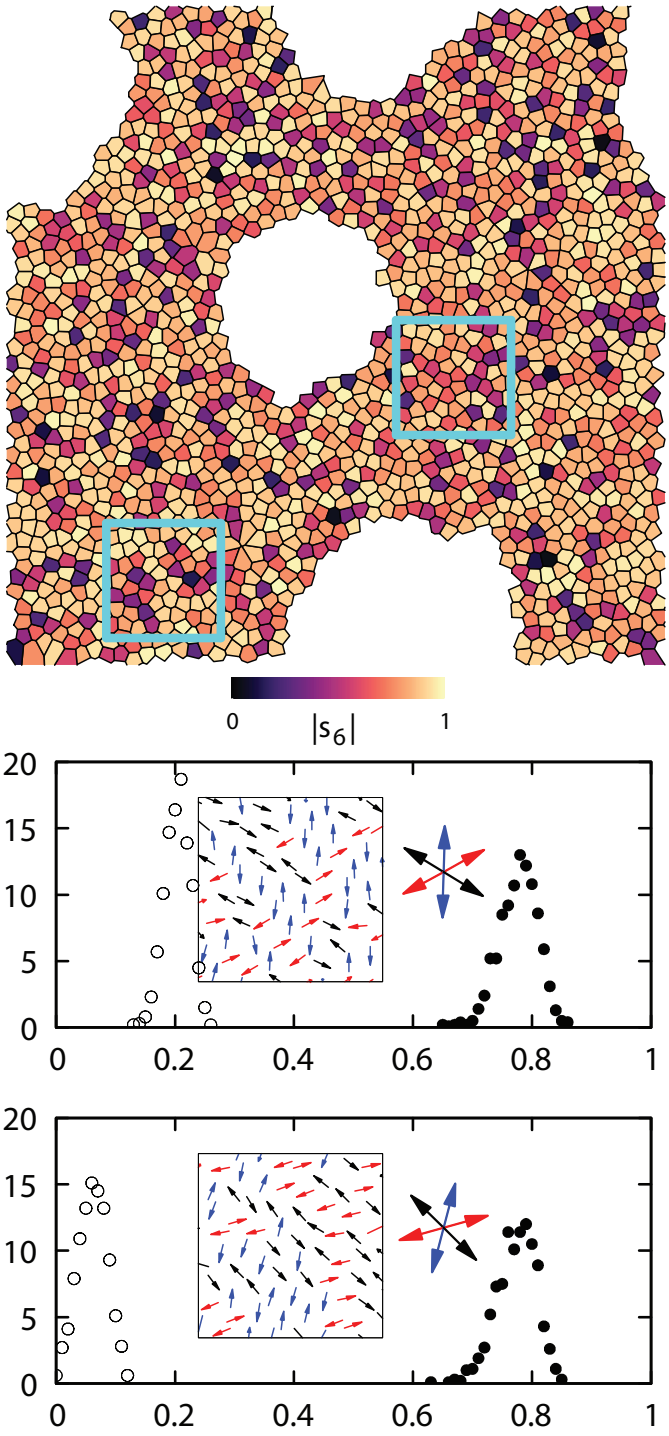

Figure 4.7: (top) Voronoi tesselation of an N=1800, T^*=0.2 system of 2dLW molecules. (bottom) Local order parameter probability density of two sections of the simulation box indicated in the top row. ψ (open circles) corresponds to bond-orientational order, and s (solid circles) corresponds to molecular-orientational order. Averages are over 1000 configurations. Inset: sections of the simulation box with molecules represented by their molecular orientation vectors, alongside the local director corresponding to that section of the simulation box.

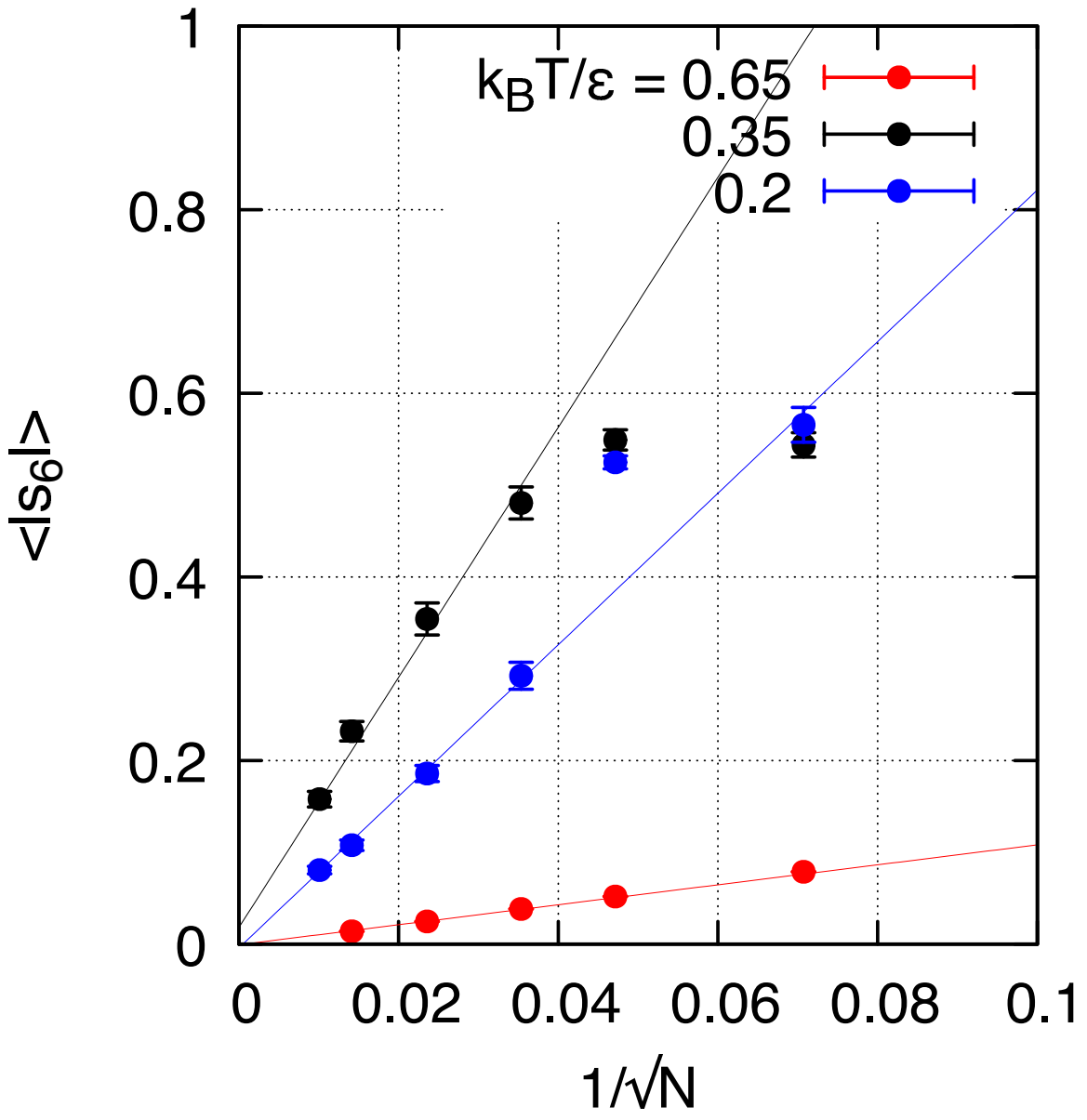

Figure 4.8: Finite size scaling of the mean of the order parameter for the 2dLW systems. Colors correspond to constant temperature, and lines are fits ignoring N = 200 and N = 450, treating the origin as a data point. Averages are taken over 100 data points of 3×10^4 configurations for a total of 3×10^6 configurations per data point. Error bars are standard error of the mean. N ranges from 200 to 9800 and is reported as $1/\sqrt{N}$ to emphasize the scaling behavior at large N.

4.3 Structural domains

We have established that six-fold MO order in the 2dLW systems is not long-range. This begs the question of obtaining a lengthscale for six-fold order. Recall $g_2(r)$, the radial distribution function, given in Equation 3.7 by

$$g_2(r) = \frac{1}{N}\frac{1}{2\pi r\rho}\left\langle \sum_j^N \sum_{k\neq j}^N \delta(r - r_{jk}) \right\rangle \tag{4.1}$$

We will abbreviate $g_2(r)$ as $g(r)$. We can also introduce a very similar function

$$g(6\theta|r) = \frac{1}{N}\frac{1}{2\pi r\rho}\left\langle \sum_j^N \sum_{k\neq j}^N \delta(r - r_{jk}) cos(6\theta_{jk}) \right\rangle \tag{4.2}$$

where θ_{jk} is the angle between the orientations of molecule j and k. We use these functions to define correlation lengths. To do so, we demand that the asymptotic form of a correlation function $h(r)$ is an eigenfunction of the ∇^2 operator. For the radial coordinate, this is the function

$$h(r/\xi) = Ce^{-r/\xi}/\sqrt{r/\xi}$$

where we introduce the correlation length ξ. In other words, we may take a linear fit to $ln\sqrt{r}h(r)$ versus r where $h(r)$ is $g(r) - g_{asymptotic}$. We identify parts of $ln\sqrt{r}h(r)$ which are qualitatively linear and compute ξ accordingly (Figures 4.9, 4.10). From these fits we table pair correlation lengths ξ and hexatic pair correlation lengths ξ_6.

k_BT/ϵ	ξ/σ	ξ_6/σ
0.65	2.1±0.9	1.0±0.8
0.4	11.18±0.08	5.31±0.07
0.35	13.0±0.5	36.8±0.2
0.2	5.8±0.9	14.2±0.1

Table 4.1: Table of correlation lengths (N=1800 2dLW). Correlation lengths are computed from a linear fit in Figures 4.9 and 4.10. Error bars are the root mean square error of the residuals from the fit. ξ is the center of mass pair correlation length, and ξ_6 is the center of mass hexatic MO pair correlation length.

The correlation lengths tell us that structural lengthscales grow in the supercooled liquid, attain their maximum at $T^* = 0.35$ near the glass transition, and shrink - not vanish - in the glass. We also learn about the temperature at which we consider the liquid deeply supercooled. Since there is only a modest increase in orientational correlation length at $T^* = 0.4$, and the orientational autocorrelation function $C_{6,s}(t)$ in Figure 3.2 shows relatively rapid relaxation, we consider temperatures colder than $T^* = 0.4$ to be deeply supercooled or glass. At and above $T^* = 0.4$ are moderately supercooled and ordinary liquids. Most importantly, correlation lengths suggest characteristic domain sizes and as such are intimately connected with many-particle dynamical processes.

4.4 Local order

We saw in Figure 4.5 that it was a useful practice to examine individual liquid configurations to seek qualitative patterns. We examined molecules and their nearest neighbors as determined by Voronoi construction to draw a schematic of local MO order in Figure 4.11. The drawings come from actual coordinates from the N=1800 2dLW trajectory files, and are colored according to the distance from the center of mass of the central molecule. The colors are meant to highlight molecular orientational order. Close inspection shows that molecules colored red ($\approx 1.7\sigma$ from the center molecule) are oriented anti-triatically $(60°, 180°, or 300°)$ from the orientation of the central molecule. On the other hand, molecules colored blue ($\approx 2.28\sigma$ from the center molecule) are oriented hexatically (multiples of 60°) from the central molecule. This observation is made quantitative in Figure 4.3(b-d). From Figure 4.3b, we see that in the systems with MO hexatic order the relative orientational angle distribution between any pair of molecules is equally and symmetrically peaked around $n \times 60°$, n an integer. Figure 4.3c shows the radial distribution of nearest neighbors as determined by Voronoi construction. Since the distribution is bimodal, we have chosen to represent nearest-neighbors using two lengthscales as indicated in the figure. The peaks of the bimodal dis-

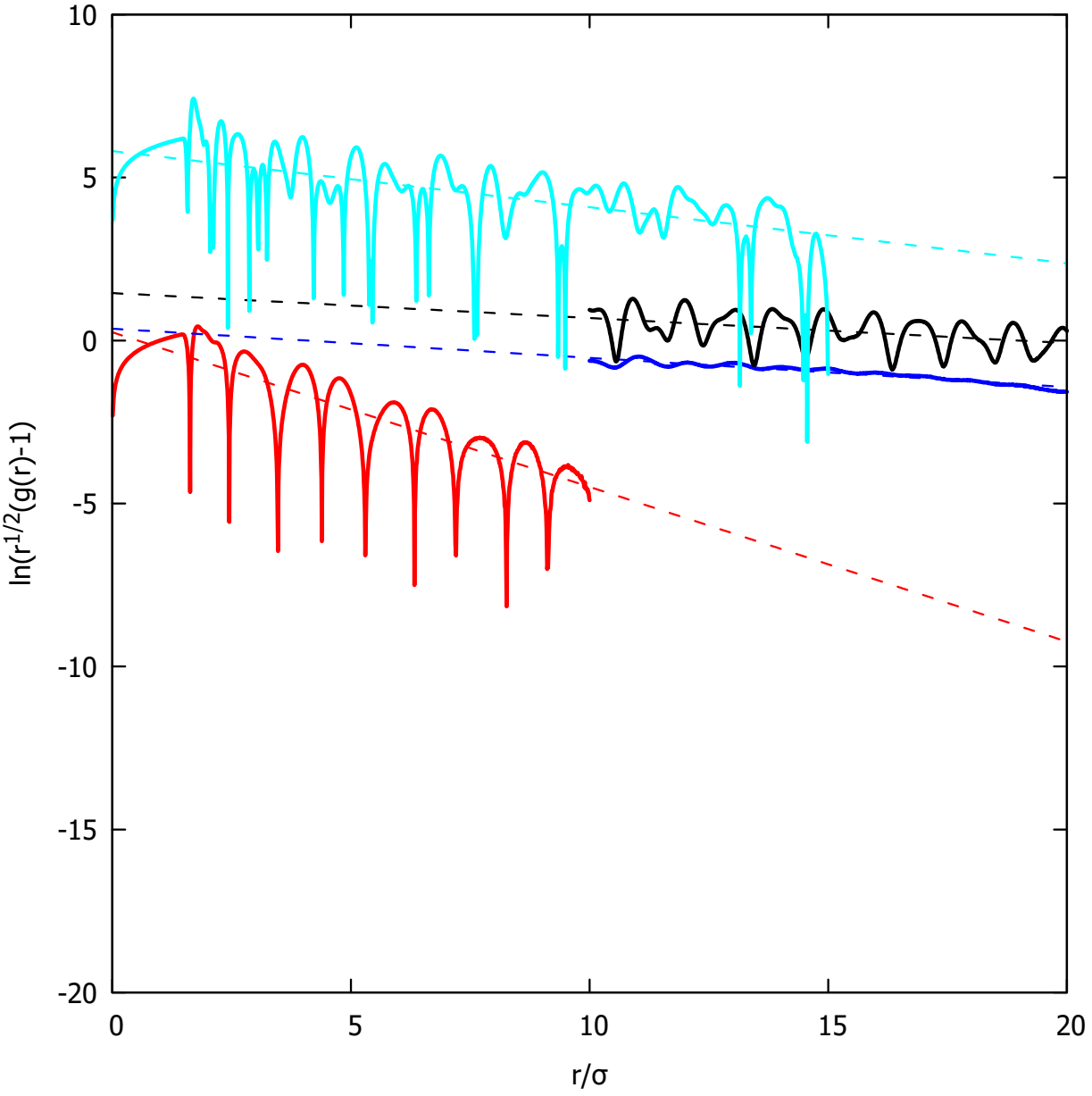

Figure 4.9: From $g(r)-1$, center of mass to center of mass correlation length ξ for the system of N=1800 molecules, zoomed in. I truncate the domain of the plot (which is the same as the domain over which the fit is taken) to avoid the noisy parts of the range. Fit parameters can be found in Table 4.3. Red, blue, black, and cyan correspond to $k_BT/\epsilon = 0.65, 0.4, 0.35, 0.2$ respectively. Curves and fits displaced vertically for visibility.

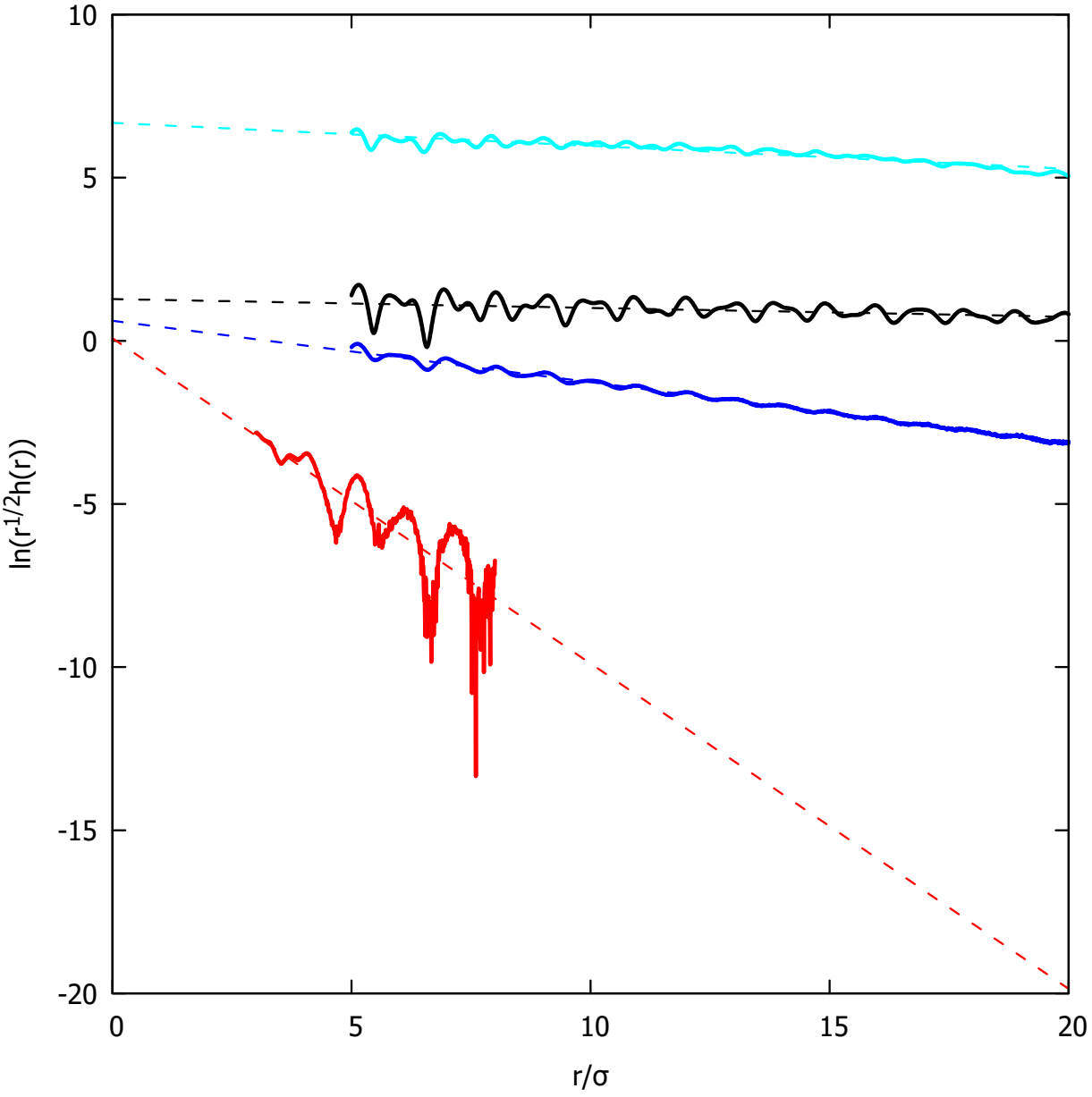

Figure 4.10: From $g(6\theta|r) - g_{asymptotic}$, center of mass to center of mass MO hexatic correlation length ξ_6 for the system of N=1800 molecules, zoomed in. $g_{asymptotic}$ is zero for most temperatures, but for the systems with global hexatic MO order it is the value of $g(6\theta|r)$ at half the box length. Red, blue, black, and cyan correspond to $k_BT/\epsilon = 0.65, 0.4, 0.35, 0.2$ respectively.

tribution are the two characteristic nearest-neighbor distances, which is corroborated by the schematic drawing in Figure 4.11. In Figure 4.3d, we study the orientational distribution of neighbors according to either lengthscale. Our findings corroborate the schematic drawing, as nearest neighbors at 1.7σ favor being anti-triatic relative to the central molecule. Nearest neighbor orientations at 2.28σ are most likely to be hexatically distributed relative to the central molecule. These two nearest-neighbor lengthscales have helped us determine what appear to be locally favorable geometries.

4.4.1 Note on cavitation

Cavitation is a known phenomenon in systems with attractive potentials, including binary glasses. [32] Cavitation describes a phenomenon in liquids where the system loses its spatial homogeneity. This occurs when the attractive interactions of particles overcome the material's tensile strength, resulting in an increase in local density throughout the system. We observe cavitation in the supercooled liquids and glasses of 2dLW (Figures 4.5, 4.1). In our constant-NVE simulations, cavitation can be understood as the system's preference for a greater density as temperature is lowered. However, the constant volume constraint of our simulation means that as local density increases, voids must form in the system - homogeneity and growth in local density are incompatible in the constant-NVE conditions. We were worried that the molecules on the edges of voids might have faster dynamics than the rest of the molecules, potentially skewing our dynamical results. To study the extent to which this is true, we studied how many molecules were on the edges of these cavities. This endeavor predated our use of cage-relative coordinates, which account for our concern that the cavities themselves may be diffusing. We have no evidence for cavity diffusion, an effect that would also be corrected for in cage-relative coordinates, but we proceeded with caution and studied the cavities in Table 4.4.1. We used Voronoi cell areas to define a criterion for whether molecules were on the edges of cavities or not. The procedure is described in the caption of Table 4.4.1. From our study of edge molecules, we conclude that there are

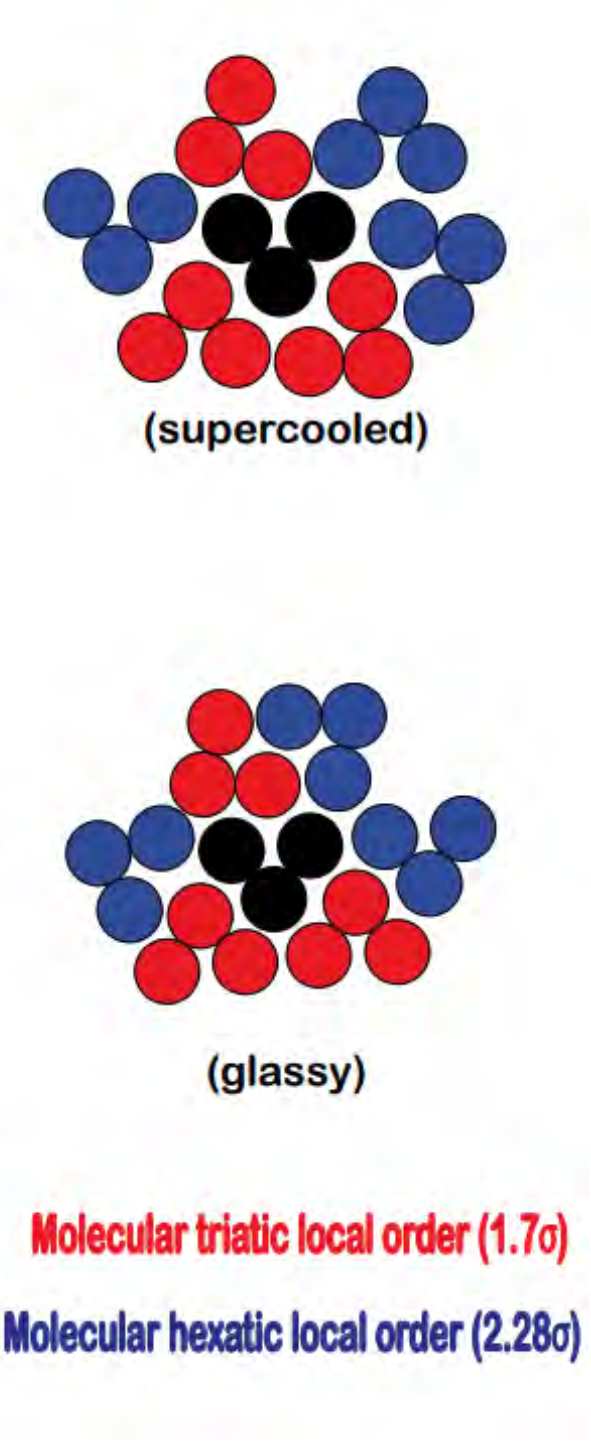

Figure 4.11: Examples of nearest-neighbor molecular orientational order. Drawings are taken from configurations of the N=1800 2dLW supercooled liquid. The central molecule is colored black, while its nearest neighbors are colored red or blue depending on the distance between the centers of mass of the central molecule and the neighbor molecule. The temperature of the supercooled example is $T^* = 0.35$, and the temperature of the glassy example is $T* = 0.2$.

relatively few edge molecules - and that the edge molecules tended to be frozen like most of the molecules in the system.

State	Molecules on edge	Peak center (σ^2)	FWHM (σ^2)
liquid	8.36 (0.46%)	3.7	1.1
supercooled	81.89 (4.55%)	3.35	0.5
glassy	116.56 (6.48%)	3.29	0.44

Table 4.2: Fraction of molecules in the system on the edge of a void. A molecule is determined to be on the edge of a void if its voronoi cell area is larger than two full-width half-maximums (FWHM) from the center of the peak of the distribution of voronoi cell areas. Probability distributions of voronoi cell areas are averaged over 100 configurations. For a normal distribution, $\int_{4\sqrt{2ln2}}^{\infty}\left[\frac{1}{\sqrt{2\pi}}e^{-x^2/2}dx\right] = 1.24\text{e-}6$, or 0.000124%. For the normal distribution, $4\sqrt{2ln2}$ is two full-width half-maxima from zero. This result is the same for gaussian distributions, so we find that two FWHM is examining behavior very, very far from the peak.

4.5 Bond-orientational order

The reason why we refer to our structure as "molecular orientational" order is due to another kind of orientational order called "bond-orientational" (BO) order. This order arose from studies of 2D melting using KTHNY theory. A good reference for BO order and 2D melting is Nelson's book. [14] BO order does not refer to chemical bonds. Rather, two particles are considered to be bonded if their Voronoi polyhedra share a face - this is equivalent to two particles being nearest neighbors. The BO order studied in 2D melting is called "hexatic" order, because bonded particles tended to have their bond-orientations hexatically distributed about a central particle. The overlap in naming convention is unfortunate and coincidental. The local BO order parameter is given by

$$\psi_{m,j} = \frac{1}{N_j}\sum_{k=1}^{N_j} e^{im\theta_k} \tag{4.3}$$

where N_j is the number of neighbors of particle j, and θ_k is the angle between the bond connecting j and k, and an arbitrary axis.

The global BO order parameter is given by

$$\psi_m = \frac{1}{N}\sum_{j=1}^{N}\psi_{m,j} \tag{4.4}$$

We also define correlation functions for MO and BO order:

$$\begin{aligned} g_m^{mo}(r) &= \big\langle cos(m(\theta(r)-\theta(0))\big\rangle \\ &= \frac{\big\langle \sum_j \sum_{k\neq j} cos(m\theta_{jk})\delta(r-r_{jk}))\big)\big\rangle}{\big\langle \sum_j \sum_{k\neq j}\delta(r-r_{jk})\big\rangle} \end{aligned} \tag{4.5}$$

$$\begin{aligned} g_m^{bo}(r) &= \big\langle \psi_6^*(0)\psi_6(r)\big\rangle \\ &= \frac{\big\langle \sum_j \sum_{k\neq j} \psi_{6,j}^*\psi_{6,k}\delta(r-r_{jk})\big\rangle}{\big\langle \sum_j \sum_{k\neq j}\delta(r-r_{jk})\big\rangle} \end{aligned} \tag{4.6}$$

These correlation functions allow us to quantitatively compare the distance-dependence of orientational order. Comparing Figures 4.12 and 4.13 indicate that triatic MO order is not very pronounced except for at short lengthscales. Hexatic MO order is not noticeable at $T* = 0.4$, but correlations become incredibly sharp only slightly colder at $T* = 0.35$. This suggests that the MO order is not yet evident by $T* = 0.4$, and one must cool further before finding these mesoscopic structures. Figure 4.14 indicates that BO order is very muted in 2dLW at all temperatures. The magnitude of the order parameter is insignificant even at short lengthscales. In light of the well-studied phenomenon of the hexatic BO ordered phase in 2D melting studies, we deduce that MO order certainly does not arise from BO order. We conjecture that perhaps MO order is suppressing BO order, since we are working in two dimensions in a temperature regime in which one would typically expect BO order.

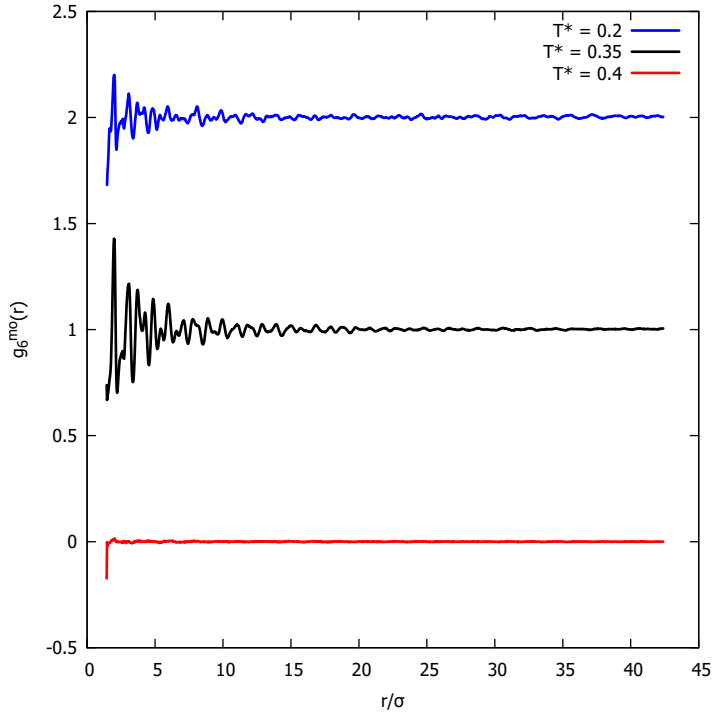

Figure 4.12: Six-fold MO correlation function for the N = 1800 systems, averaged over 3×10^5 configurations. Curves displaced vertically for visual clarity.

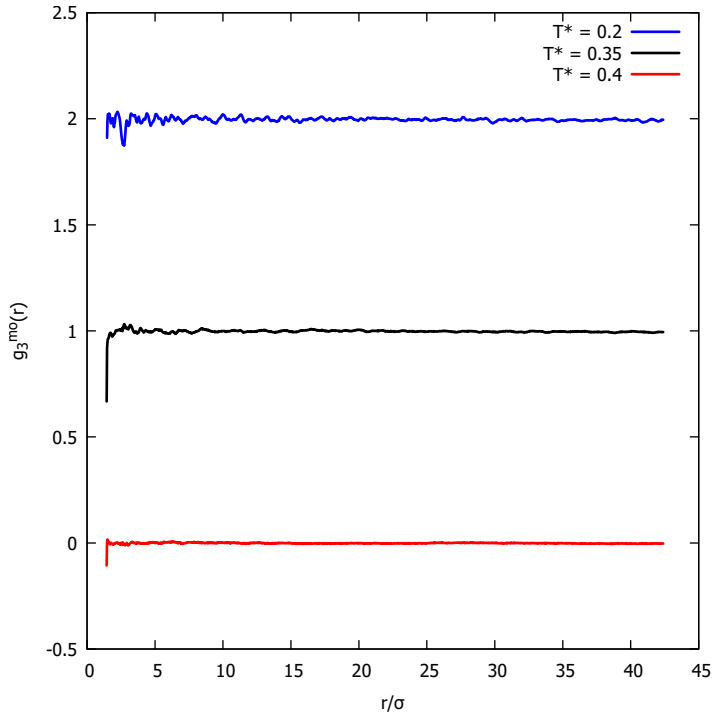

Figure 4.13: Three-fold MO correlation function for the N = 1800 systems, averaged over 3×10^5 configurations. Curves displaced vertically for visual clarity.

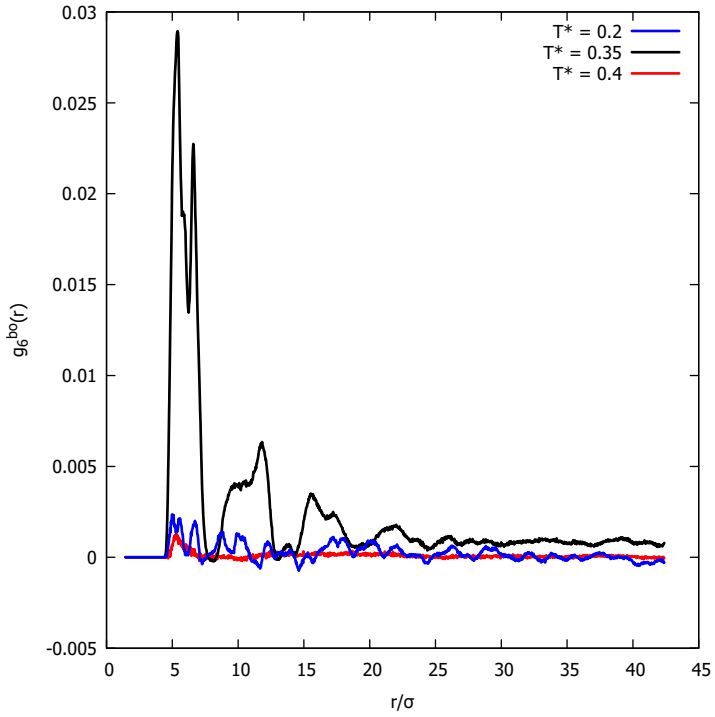

Figure 4.14: Hexatic BO correlation function for the N = 1800 systems, averaged over 3×10^5 configurations. Note that the scale in this figure is much smaller than that of Figures 4.12 and 4.13.

CHAPTER 5

Conclusion

This thesis began by setting up the anomalously slow dynamical phenomena in supercooled liquids in general. We proposed a two-dimensional model to successfully capture these dynamical phenomena, but came to a surprising finding that the liquid upon supercooling attained high degrees of symmetry in the form of locally ordered domains. The focus of this thesis shifted from a purely dynamical study to one trying to understand the implications of clear structural order in the midst of supercooling, in direct contrast to literature expectations about the equivalence between supercooled liquid and ordinary liquid structure.

An important task was to separate our molecular-orientational hexatic order from the well-known 2d phenomenon of bond-orientational hexatic order. It is not difficult to imagine how bond-orientational order might enforce molecular-orientational order. We establish that this is not the case in our simulations, as we find in the supercooled liquid that bond-orientational correlations were too small in magnitude and decayed too quickly to be related to the bond-orientational order of 2d melting. Rather than finding significant local bond-orientational order, we actually find different kinds of local molecular-orientational ordering. Upon supercooling, two nearest-neighbor lengthscales arise. One lengthscale, 1.7σ, is dominated by anti-triatic molecular orientational order relative to the central molecule, where

neighboring molecules' orientations are 60, 180, or 300 degrees out of phase with respect to the central molecule. The other lengthscale, 2.28σ, features true hexatic molecular orientational order. It would be an interesting focus of future study to determine the relationship between this nearest-neighbor ordering with a lengthscale of about a particle's length, to the mesoscopic ordering we find with a lengthscale as long as dozens of particles' lengths.

Our findings about domains indicate that structure is an important consideration in the study of supercooled liquids. Our study is limited in that we only examine one model supercooled liquid in detail, with an incomplete study of other models in Appendix A. In light of the experimental and theoretical work on hard triangles of various symmetries that find phases with hexatic molecular-orientational order, we ponder whether m-adic molecular-orientational order ($m \neq 1, 2$) occurs in other, more realistic physical systems like ours. [15] [31] We note that neither of these studies made a connection between their molecular-orientational order and glassy dynamics. In particular, we would be interested to see whether molecular-orientational order has existed all along in molecular glassformers and simply has gone unnoticed until now. If not, we are interested to know what aspects of our model give rise to molecular-orientational order.

Whether molecular-orientational order is present in all glassformers or not, our results have further implications. The exact mechanism of domain formation may not be important. What is more likely to be fundamental to glassy dynamics is the fact that domains form at all. This thesis presents evidence that links domain formation to supercooled dynamics, which suggests that future studies look to local ordering processes in order to find structural signatures of glassy phenomena. That the 2dLW supercooled liquid is perfectly described by the drastic divergence of relaxation times modeled by the VFT law all while sustaining ordered domains indicates at the very least that supercooled liquids are capable of supporting structural order. It remains to be shown the exact nature of this link between structure and order, but certainly in our study the two are very much compatible. Our work suggests just one microscopic example of domain formation. Future work may determine whether our

example is archetypal of domain formation in supercooled liquids. In any case, we hope our work leads the way to bridging structure and dynamics in supercooled liquids.

APPENDIX A

Results from other trimer models

We also conducted studies on models obtained by varying the apical angle in the 2dLW model. In addition to the 75° angle, we conducted simulations on $N = 800$ trimer molecules with angle $45, 55, 65, 85, 95, 105$ degrees. The aim of these simulations were to determine whether other trimer models attained some degree of molecular-orientational order. s_m for $m = 1, 2, 3, 4, 5, 6, 8$ and $g_2(r)$ were computed from these simulations. We summarize the results here in Table A.1. These studies are incomplete, but contain important information that will inform future work.

The following figures are $g_2(r)$ and $P(s_m)$ data from these non-75° studies. All high

angle (degrees)	lattice?	nontrivial order	comment
45	no	s_6, s_8	broader-than-expected distributions near zero
55	yes	s_6, s_8	
65	yes	none	
85	no	none	
95	no	none	
105	no	s_1, s_2, s_4, s_6, s_8	sharp distributions at small, nonzero s_m

Table A.1: Summary of structural results obtained for N = 800 simulations of trimer models with the same parameters as 2dLW except for the listed apical angle. Presence of a lattice is determined qualitatively using $g_2(r)$, and nontrivial order is determined using the probability distribution of global order parameters s_m.

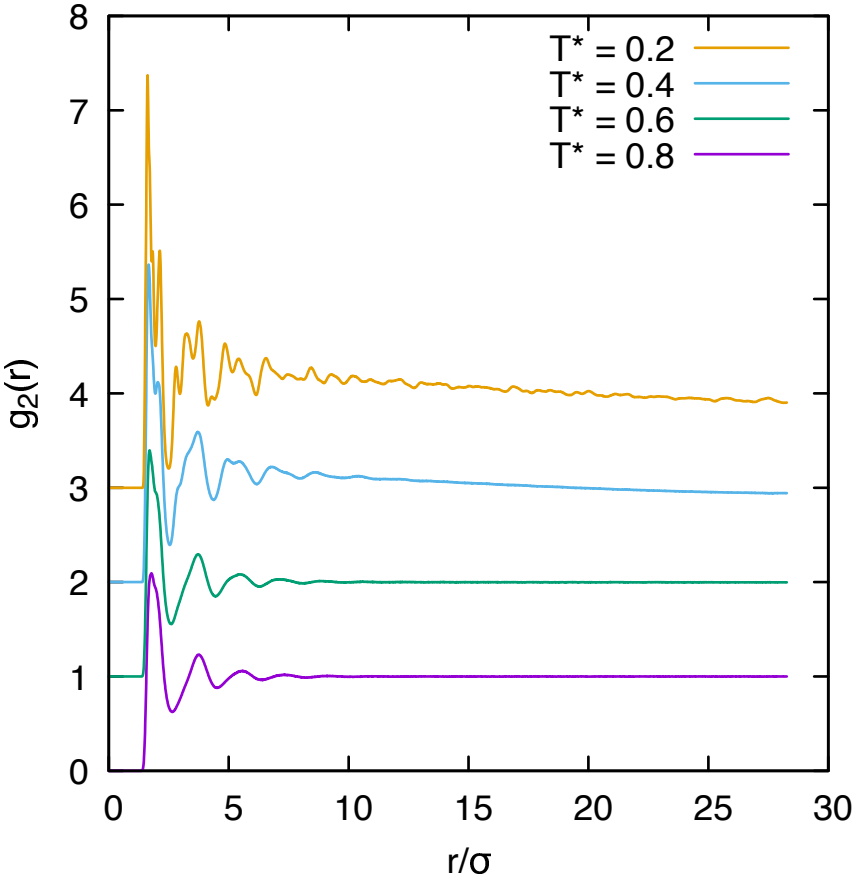

Figure A.1: Radial distribution function obtained from N = 800 simulations of 45° trimers. Results are averaged over 3×10^4 configurations. The simulation runs are started up using the same procedures we used for 2dLW, described in Chapter 2. Distances are measured between centers of mass of molecules. Curves are displaced vertically for visual clarity.

temperature $T* = 0.8, 0.6$ results for $P(s_m)$ are omitted. The $g_2(r)$ plots are mostly uninteresting, but we will show the $45°, 55°, 105°$ results and omit the rest. The temperature progression of $g_2(r)$ for 45° and 105° represent well the $g_2(r)$ for other models labeled "no lattice" in Table A.1, and likewise for 55° and "yes lattice".

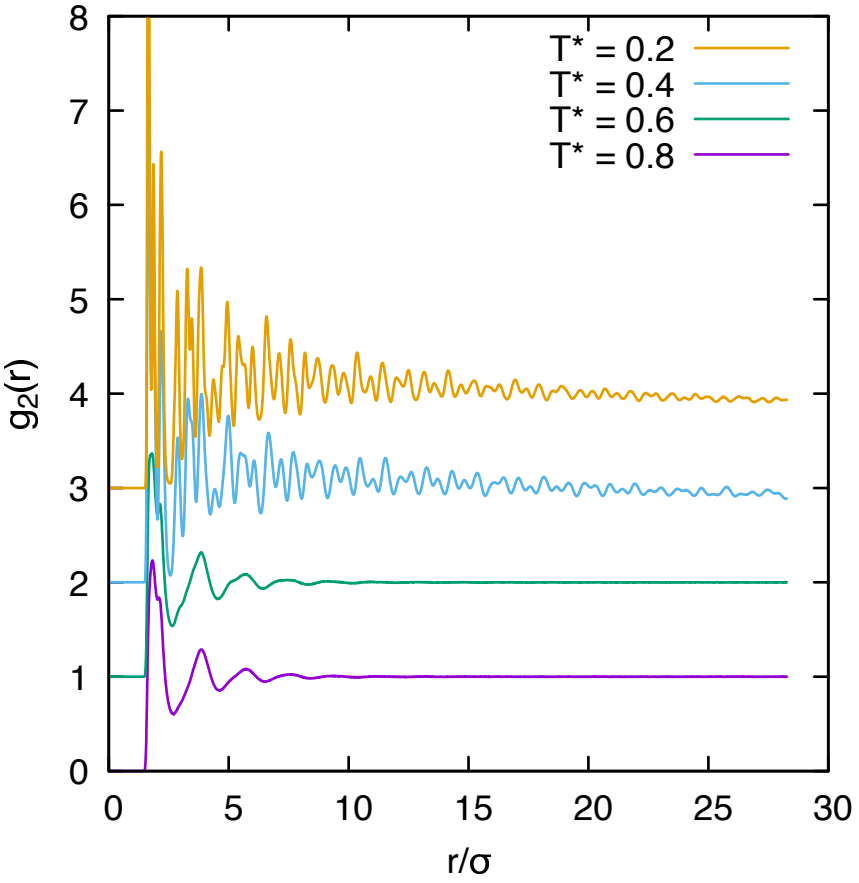

Figure A.2: Radial distribution function obtained from N = 800 simulations of 55° trimers. Results are averaged over 3×10^4 configurations. The simulation runs are started up using the same procedures we used for 2dLW, described in Chapter 2. Distances are measured between centers of mass of molecules. Curves are displaced vertically for visual clarity.

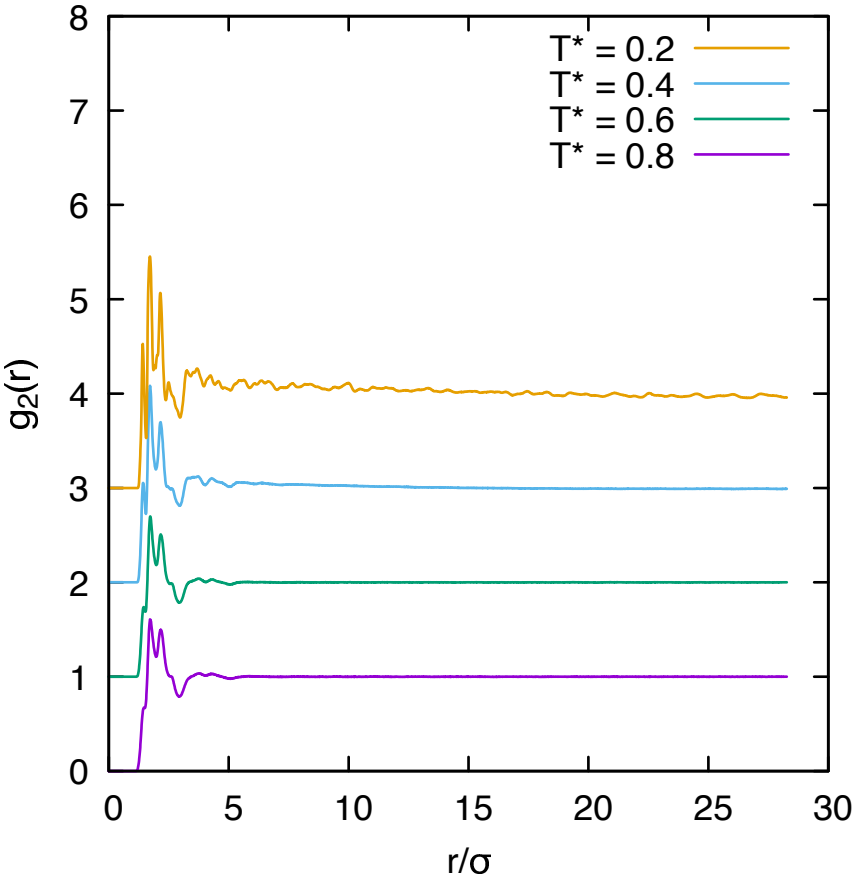

Figure A.3: Radial distribution function obtained from N = 800 simulations of 105° trimers. Results are averaged over 3×10^4 configurations. The simulation runs are started up using the same procedures we used for 2dLW, described in Chapter 2. Distances are measured between centers of mass of molecules. Curves are displaced vertically for visual clarity.

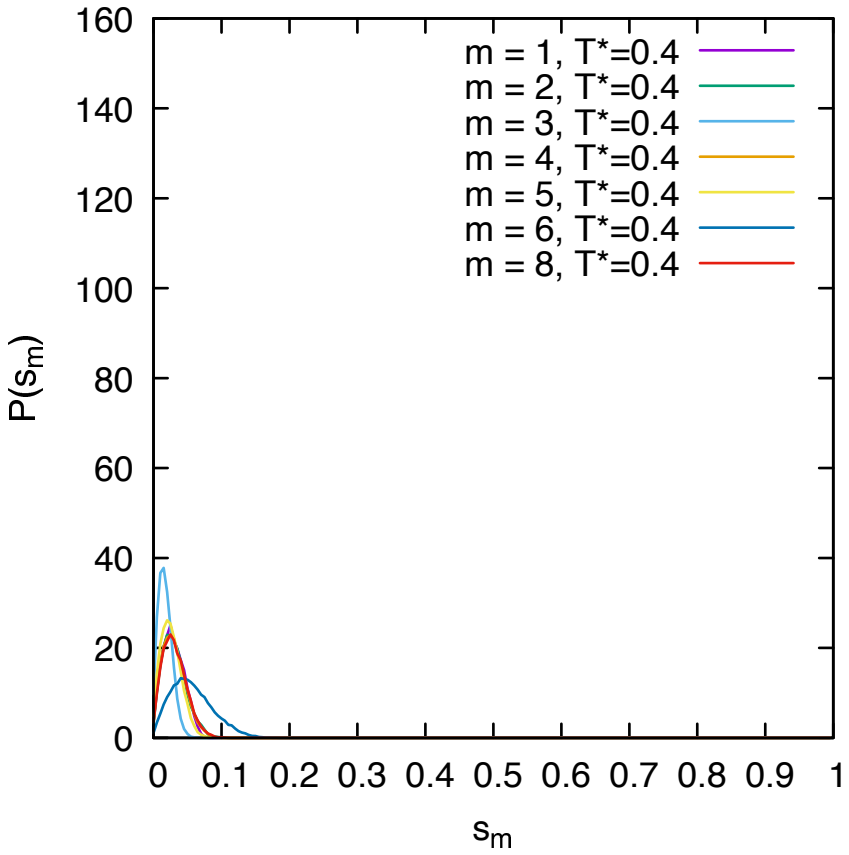

Figure A.4: Probability distribution of the order parameter s_m in N = 800 simulations of 45° trimers. Results are averaged over 3×10^4 configurations. The simulation runs are started up using the same procedures we used for 2dLW, described in Chapter 2.

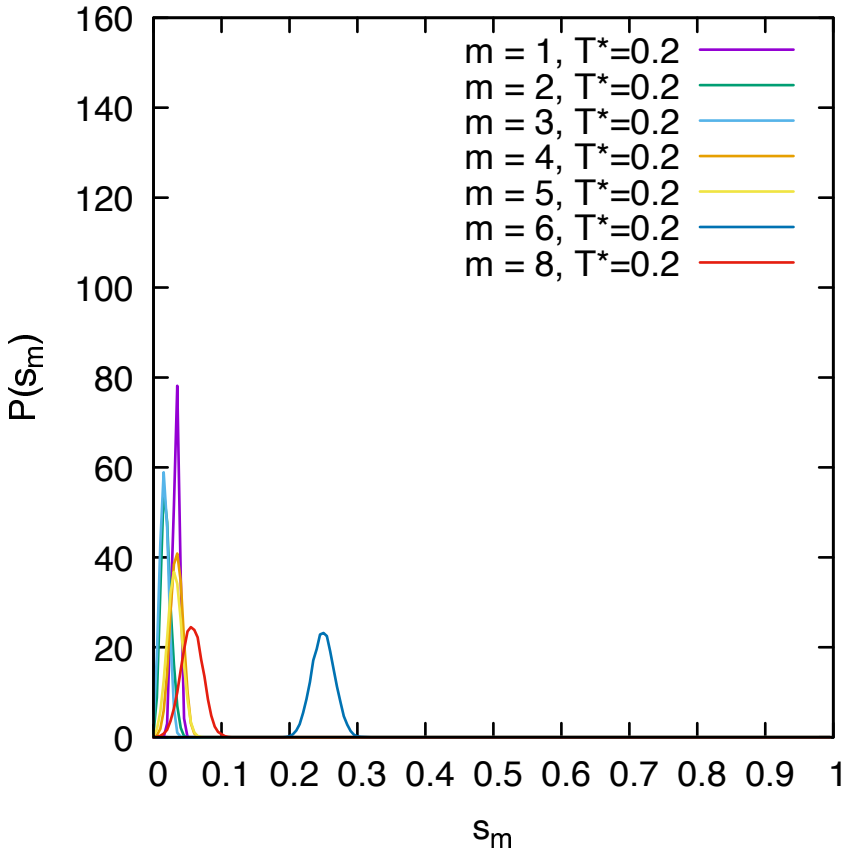

Figure A.5: Probability distribution of the order parameter s_m in N = 800 simulations of 45° trimers.

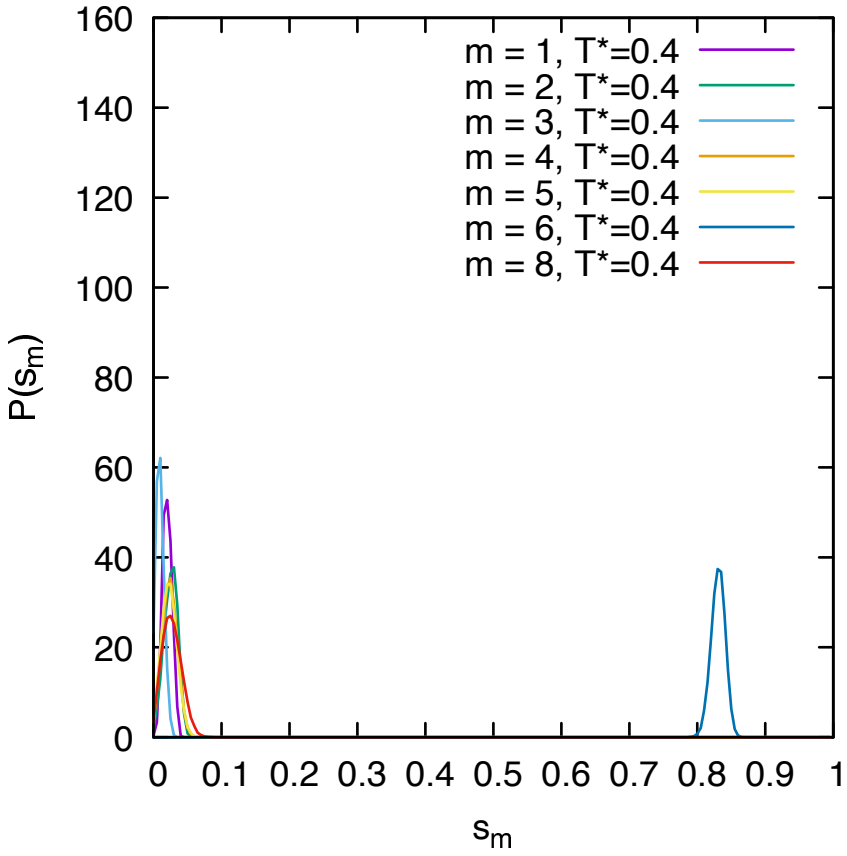

Figure A.6: Probability distribution of the order parameter s_m in N = 800 simulations of 55° trimers.

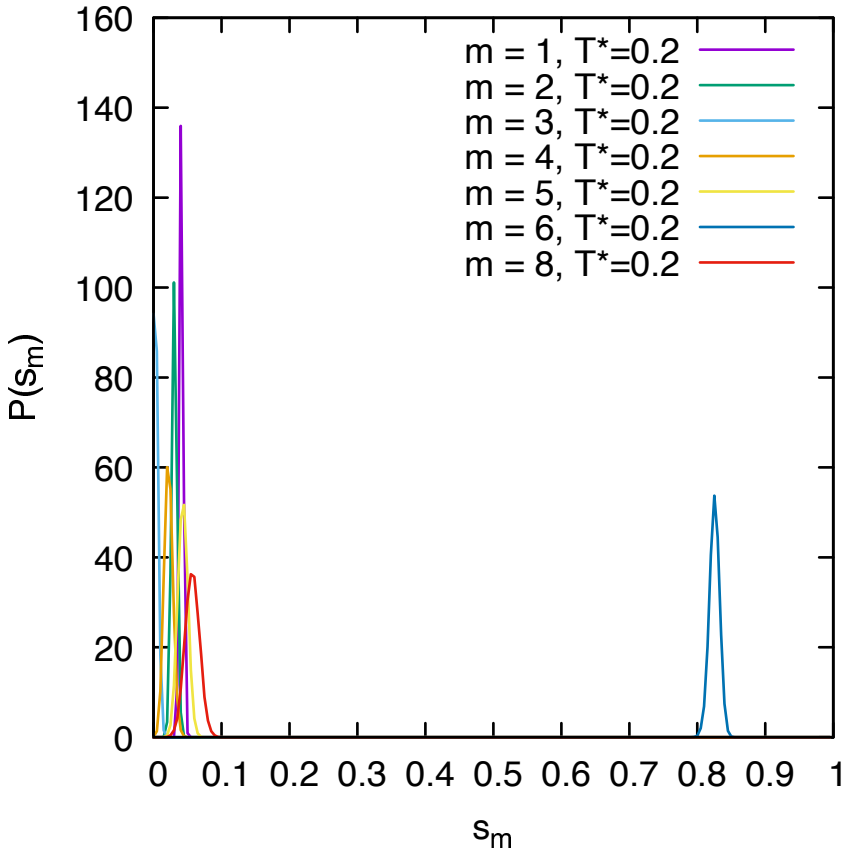

Figure A.7: Probability distribution of the order parameter s_m in N = 800 simulations of 55° trimers.

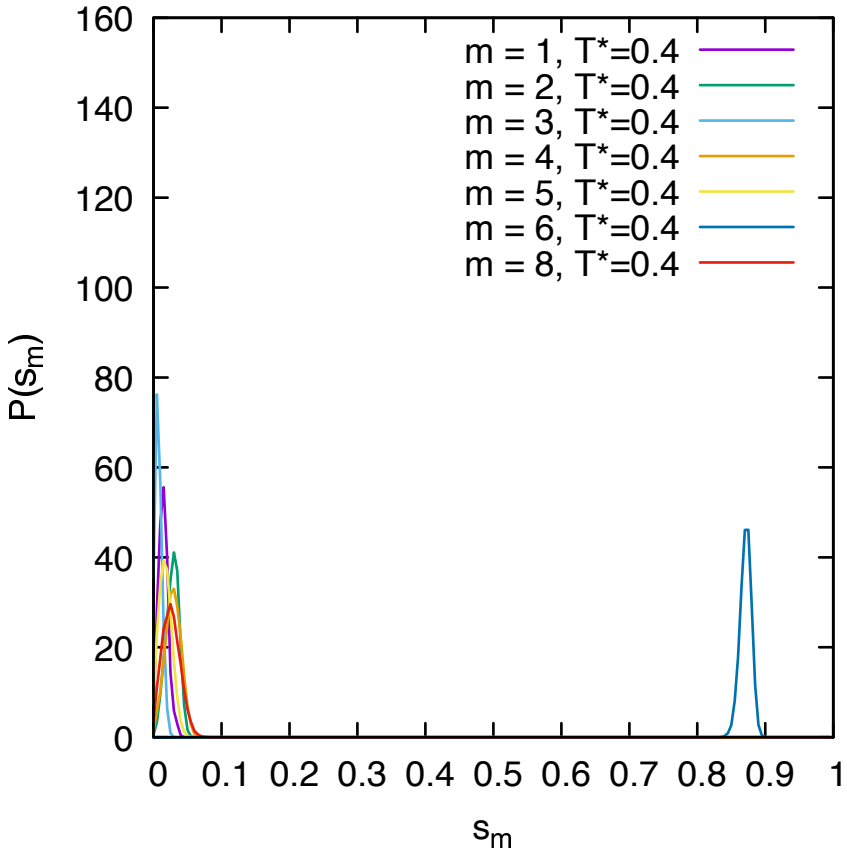

Figure A.8: Probability distribution of the order parameter s_m in N = 800 simulations of 65° trimers.

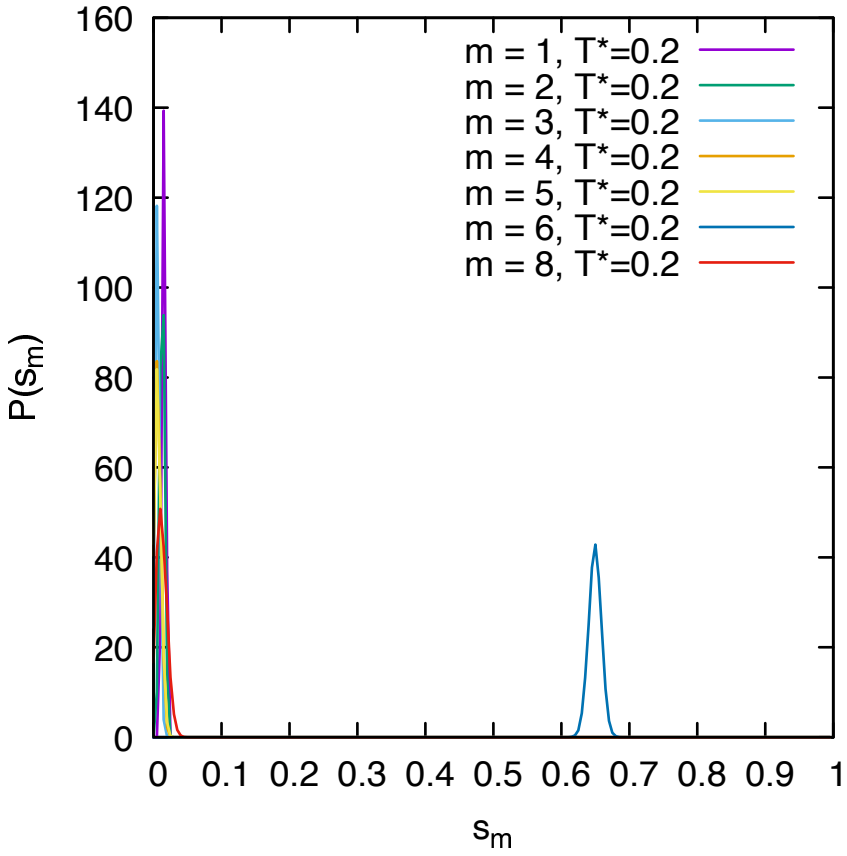

Figure A.9: Probability distribution of the order parameter s_m in N = 800 simulations of 65° trimers.

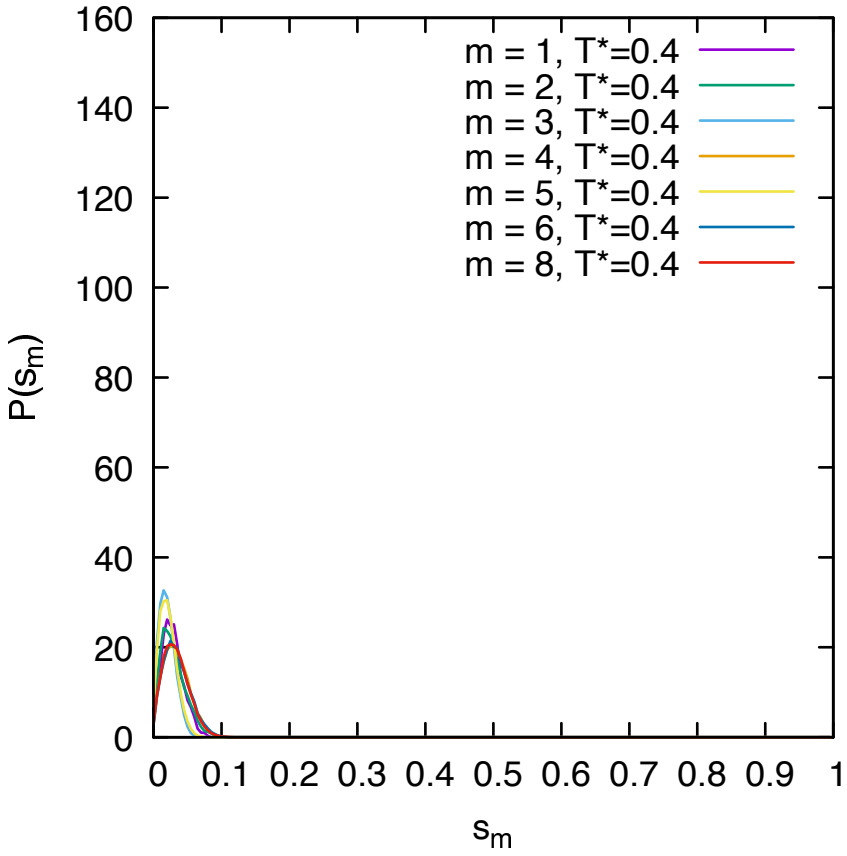

Figure A.10: Probability distribution of the order parameter s_m in N = 800 simulations of 85° trimers.

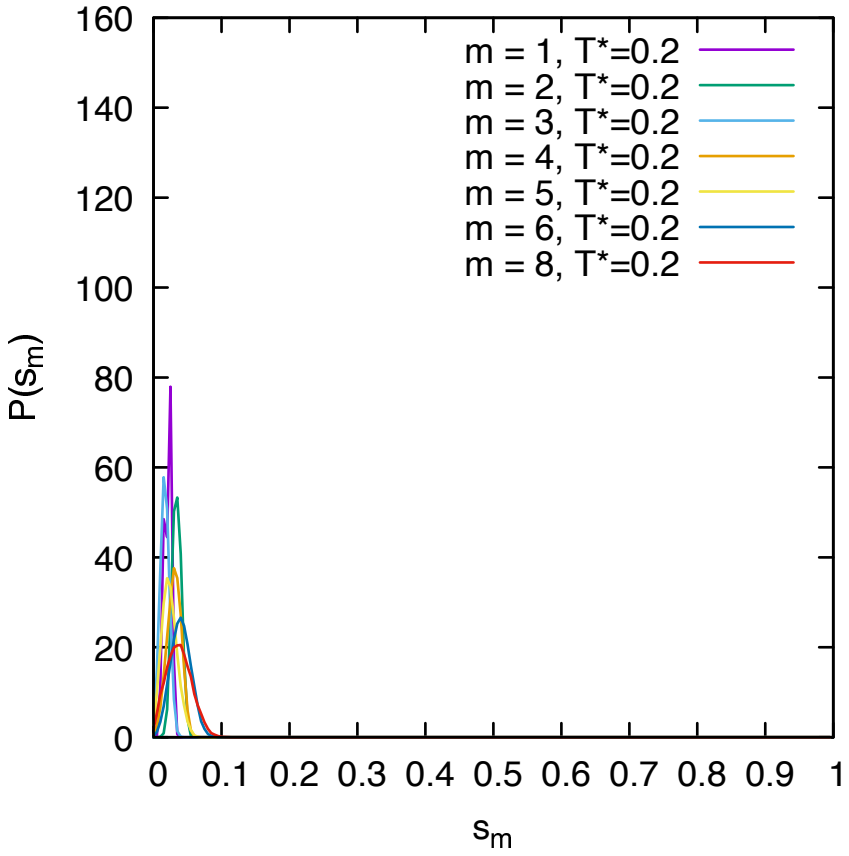

Figure A.11: Probability distribution of the order parameter s_m in N = 800 simulations of 85° trimers.

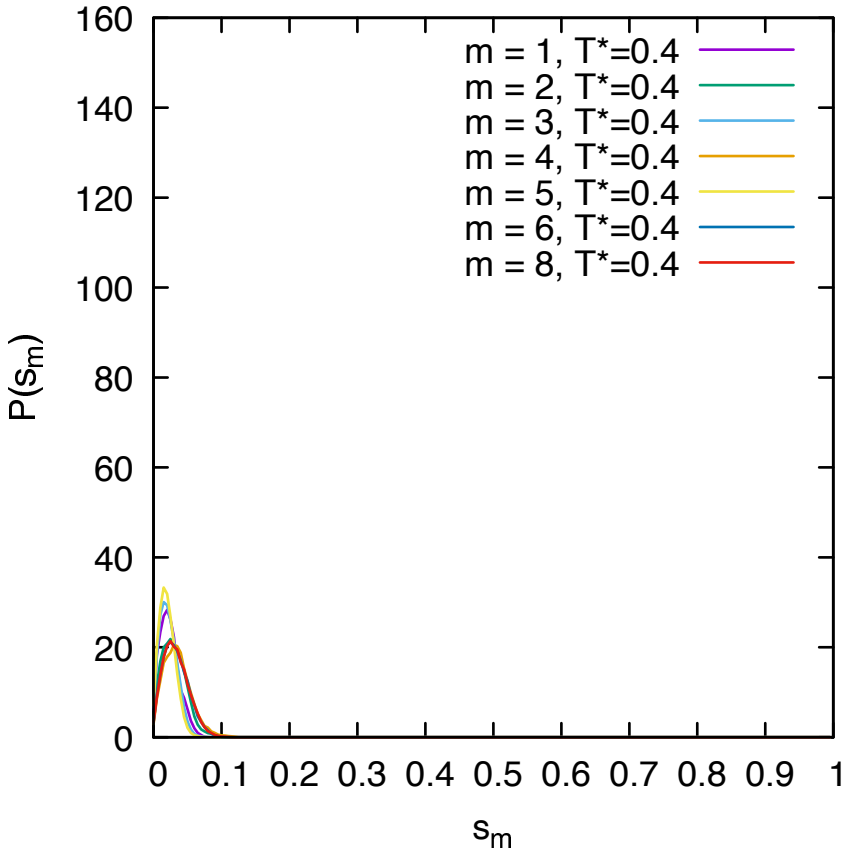

Figure A.12: Probability distribution of the order parameter s_m in N = 800 simulations of 95° trimers.

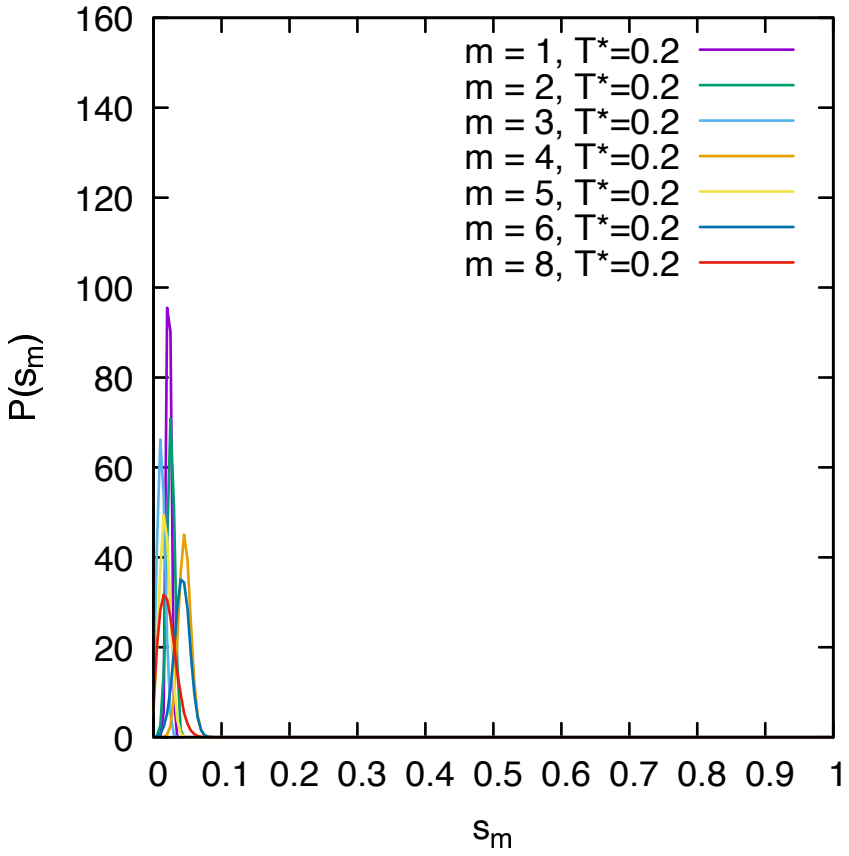

Figure A.13: Probability distribution of the order parameter s_m in N = 800 simulations of 95° trimers.

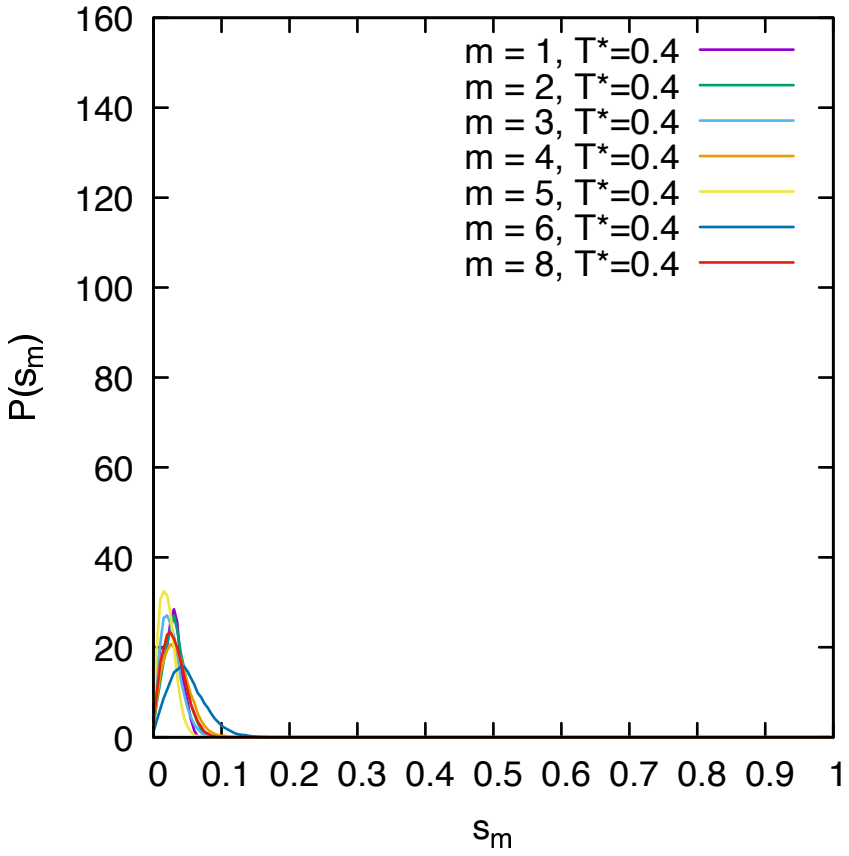

Figure A.14: Probability distribution of the order parameter s_m in N = 800 simulations of 105° trimers.

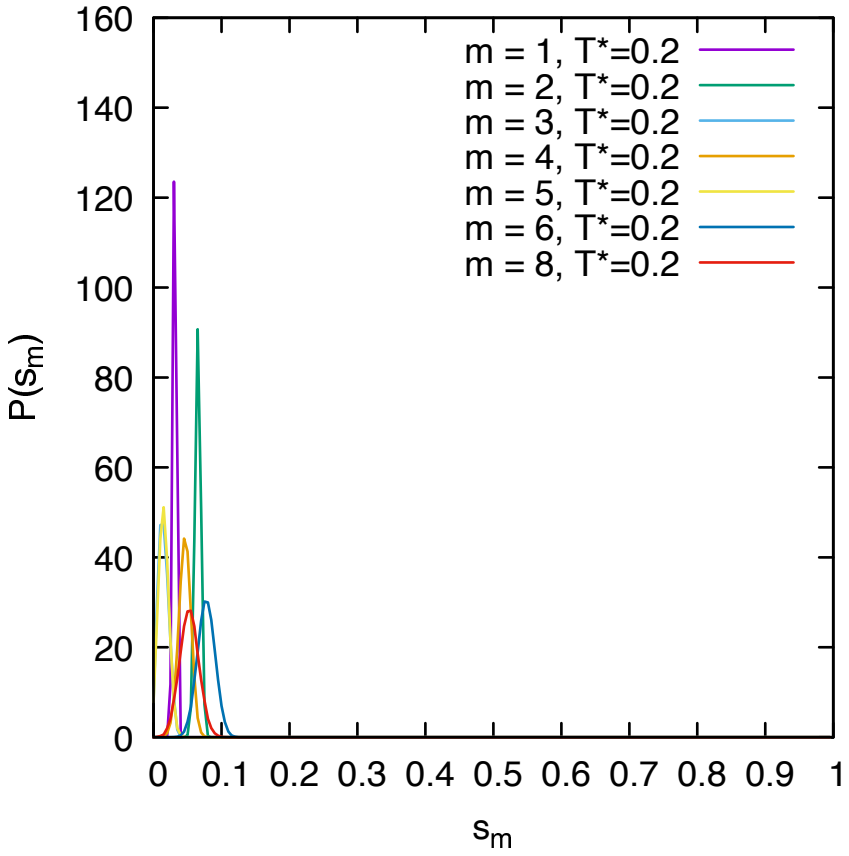

Figure A.15: Probability distribution of the order parameter s_m in N = 800 simulations of 105° trimers.

Bibliography

[1] Daniel Cressey and Ewen Callaway. Cryo-electron microscopy wins chemistry nobel. *Nature News*, 550(7675):167, 2017.

[2] Yrjö H Roos. Glass transition temperature and its relevance in food processing. *Annual Review of Food Science and Technology*, 1:469–496, 2010.

[3] Masao Doi. *Soft matter physics*. Oxford University Press, 2013.

[4] Andrea Cavagna. Supercooled liquids for pedestrians. *Physics Reports*, 476(4-6):51–124, 2009.

[5] Pierre-Gilles de Gennes. Soft matter (nobel lecture). *Angewandte Chemie International Edition in English*, 31(7):842–845, 1992.

[6] Pierre-Gilles De Gennes and Jacques Prost. *The physics of liquid crystals*, volume 83. Oxford university press, 1993.

[7] Ludovic Berthier and Giulio Biroli. Theoretical perspective on the glass transition and amorphous materials. *Reviews of Modern Physics*, 83(2):587, 2011.

[8] Hu Cang, Jie Li, VN Novikov, and MD Fayer. Dynamics in supercooled liquids and in the isotropic phase of liquid crystals: A comparison. *The Journal of chemical physics*, 118(20):9303–9311, 2003.

[9] Elijah Flenner and Grzegorz Szamel. Fundamental differences between glassy dynamics in two and three dimensions. *Nature communications*, 6(1):1–6, 2015.

[10] Bernd Illing, Sebastian Fritschi, Herbert Kaiser, Christian L Klix, Georg Maret, and Peter Keim. Mermin–wagner fluctuations in 2d amorphous solids. *Proceedings of the National Academy of Sciences*, 114(8):1856–1861, 2017.

[11] Skanda Vivek, Colm P Kelleher, Paul M Chaikin, and Eric R Weeks. Long-wavelength fluctuations and the glass transition in two dimensions and three dimensions. *Proceedings of the National Academy of Sciences*, 114(8):1850–1855, 2017.

[12] Hayato Shiba, Yasunori Yamada, Takeshi Kawasaki, and Kang Kim. Unveiling dimensionality dependence of glassy dynamics: 2d infinite fluctuation eclipses inherent structural relaxation. *Physical review letters*, 117(24):245701, 2016.

[13] N David Mermin and Herbert Wagner. Absence of ferromagnetism or antiferromagnetism in one-or two-dimensional isotropic heisenberg models. *Physical Review Letters*, 17(22):1133, 1966.

[14] David R Nelson. *Defects and geometry in condensed matter physics*. Cambridge University Press, 2002.

[15] Kun Zhao, Robijn Bruinsma, and Thomas G Mason. Local chiral symmetry breaking in triatic liquid crystals. *Nature communications*, 3(1):1–8, 2012.

[16] Michael P Allen and Dominic J Tildesley. *Computer simulation of liquids*. Oxford university press, 2017.

[17] David R Reichman and Patrick Charbonneau. Mode-coupling theory. *Journal of Statistical Mechanics: Theory and Experiment*, 2005(05):P05013, 2005.

[18] Giulio Biroli and Jean-Philippe Bouchaud. The random first-order transition theory of glasses: A critical assessment. *Structural Glasses and Supercooled Liquids: Theory, Experiment, and Applications*, pages 31–113, 2012.

[19] Laurent J Lewis and Göran Wahnström. Molecular-dynamics study of supercooled ortho-terphenyl. *Physical Review E*, 50(5):3865, 1994.

[20] S Mossa, E La Nave, HE Stanley, C Donati, F Sciortino, and P Tartaglia. Dynamics and configurational entropy in the lewis-wahnström model for supercooled orthoterphenyl. *Physical Review E*, 65(4):041205, 2002.

[21] Adele Rinaldi, Francesco Sciortino, and Piero Tartaglia. Dynamics in a supercooled molecular liquid: Theory and simulations. *Physical Review E*, 63(6):061210, 2001.

[22] Ulf R Pedersen, Toby S Hudson, and Peter Harrowell. Crystallization of the lewis–wahnström ortho-terphenyl model. *The Journal of chemical physics*, 134(11):114501, 2011.

[23] Hans C Andersen. Rattle: A "velocity" version of the shake algorithm for molecular dynamics calculations. *Journal of Computational Physics*, 52(1):24–34, 1983.

[24] Hiroshi Shintani and Hajime Tanaka. Frustration on the way to crystallization in glass. *Nature Physics*, 2(3):200–206, 2006.

[25] Jean-Pierre Hansen and Ian R McDonald. *Theory of simple liquids*. Elsevier, 1990.

[26] C Austen Angell. Formation of glasses from liquids and biopolymers. *Science*, 267(5206):1924–1935, 1995.

[27] Yan Zhao and Richard M Stratt. Measuring order in disordered systems and disorder in ordered systems: Random matrix theory for isotropic and nematic liquid crystals and its perspective on pseudo-nematic domains. *The Journal of chemical physics*, 148(20):204501, 2018.

[28] Daniele Coslovich and Giorgio Pastore. Understanding fragility in supercooled lennard-jones mixtures. i. locally preferred structures. *The Journal of chemical physics*, 127(12):124504, 2007.

[29] Jonathan PK Doye, David J Wales, Fredrik HM Zetterling, and Mikhail Dzugutov. The favored cluster structures of model glass formers. *The Journal of chemical physics*, 118(6):2792–2799, 2003.

[30] Mikhail Dzugutov, Sergei I Simdyankin, and Fredrik HM Zetterling. Decoupling of diffusion from structural relaxation and spatial heterogeneity in a supercooled simple liquid. *Physical review letters*, 89(19):195701, 2002.

[31] Yuri Martínez-Ratón, Ariel Díaz-De Armas, and Enrique Velasco. Uniform phases in fluids of hard isosceles triangles: One-component fluid and binary mixtures. *Physical Review E*, 97(5):052703, 2018.

[32] Y Elia Altabet, Andreia L Fenley, Frank H Stillinger, and Pablo G Debenedetti. Cavitation transition in the energy landscape: Distinct tensile yielding behavior in strongly and weakly attractive systems. *The Journal of chemical physics*, 148(11):114501, 2018.